Journal of Environmental Chemical Engineering 11 (2023) 111378

Contents lists available at ScienceDirect

Journal of Environmental Chemical Engineering

journal homepage: www.elsevier.com/locate/jece

Separation of CO_2 using biochar and KOH and $ZnCl_2$ activated carbons derived from pine sawdust

Catarina Helena Pimentel, Lidia Díaz-Fernández, Diego Gómez-Díaz, María Sonia Freire, Julia González-Álvarez *

Department of Chemical Engineering, School of Engineering, Universidade de Santiago de Compostela, Santiago de Compostela 15782, Spain

ARTICLE INFO

Editor:Dong-Yeun Koh

Keywords:
Activated carbon
Pine sawdust
CO_2 adsorption
Isotherm models
CO_2/N_2 selectivity
Heat of adsorption

ABSTRACT

Due to the CO_2 emissions and greenhouse effect, reducing its harmful impacts on climatic conditions is necessary. CO_2 adsorption in a microporous carbon structure is one of the more effective separation techniques to avoid this type of emissions. In this work, one biochar (BC) and five activated carbons (ACs) were produced from *Pinus radiata* sawdust by chemical activation with potassium hydroxide (KOH) or zinc chloride ($ZnCl_2$). Characterization was performed by scanning and transmission electron microscopy (SEM and TEM), surface area and pore size distribution by volumetric N_2 and CO_2 adsorption experiments using the Brunauer-Emmet-Teller (BET) and Barret-Joyner-Halenda (BJH) methods, respectively, X-ray diffraction (XRD), elemental analysis and X-ray photoelectron spectroscopy (XPS). The performance efficiency of the carbons was analyzed in terms of CO_2 adsorption capacity at an absolute pressure range of 0–760 mmHg and at different temperatures (0, 25 and 50 °C). The apparent and IAST selectivity of CO_2 over N_2 were determined and all carbons showed preferential sorption for CO_2. Langmuir, Freundlich and Toth isotherms were employed to analyze pure CO_2 and N_2 adsorption data and the Toth isotherm gave the best fit. The carbon activated at 600°C with KOH at a ratio of 1:4 w/w achieved the largest CO_2 uptake (5.79 mmol/g at 0 °C and 750 mmHg) due to a combination between high microporosity (89 %) and surface area (2437 m^2/g). This carbon also reached a relatively high selectivity.

1. Introduction

One of the most anthropogenic greenhouse gases (GHG) having a detrimental impact on the environment and associated to climate change is carbon dioxide (CO_2), contributing more than 60 % to global warming. Then, reduction of CO_2 emissions, which in the recent years has been one of the main efforts of the scientific community [1–3], is of great importance. Since the concentration of CO_2 continues to increase it is essential to reduce the carbon footprint in most countries and search for solutions and alternatives for more sustainable forms of energy. Meanwhile, as fossil fuel (coal, natural gas and oil) burning is still the primary energy supply it is crucial to develop carbon capture with low energy penalty and storage technologies (CCS) to deal with the global challenge of CO_2 reduction [4].

Nowadays, the most common technique used in industry for CO_2 capture is chemical absorption with monoethanolamine (MEA) since it is relatively cheap, easily available and a fast reaction occurs with CO_2. However, several disadvantages can be mentioned such as high energy requirements for the regeneration and recycling of the solvent, equipment corrosion and solvent degradation [2,4]. This highlights the importance of using economically viable technologies. Adsorption, as a less expensive technique, ease of handling, presenting a good capturing capacity, high selectivity, extended stability, with lower energy requirements for regeneration and recycling and fast kinetics, represents a promising alternative [5]. Therefore, extensive research has been made to prepare efficient CO_2 adsorbents, such as carbonaceous materials, zeolites, metal organic frameworks (MOFs), clays, alkali-metal based materials, amine loaded materials and nitrogen-rich microporous polymers [1,6]. However, due to economical and/or technical issues some of these materials are still far from large-scale application [2].

The selection of a good adsorbent implies to consider both the type of material (i.e., hydrophobicity, acidity, etc.) and the pore size of the target adsorbent. Particularly, in the case of CO_2 the microporous region (< 2 nm) is the most important one since it is known to be favorable for CO_2 adsorption. Moreover, the importance of the ultra-micropores (< 0.7 nm) for CO_2 adsorption has been emphasized [7]. Additionally, high

* Correspondence to: School of Engineering, Rúa Lope Gómez de Marzoa s/n, 15782 Santiago de Compostela, Spain.
E-mail address: julia.gonzalez@usc.es (J. González-Álvarez).

https://doi.org/10.1016/j.jece.2023.111378
Received 9 June 2023; Received in revised form 11 August 2023; Accepted 29 October 2023
Available online 2 November 2023

adsorption capacity, high CO_2/N_2 selectivity, low affinity to impurities, regeneration ability, mechanical and thermal stability are also essential characteristics [4]. Most notably, porous carbons revealed to be very competitive adsorbents due to their properties such as high specific area, porous structure, favorable surface chemistry, high chemical and thermal stability, reversibility and high recyclability [1].

In the context of circular economy and sustainable development and as commercial activated carbons normally show low CO_2 adsorption capacity, the synthesis of carbons from renewable inexpensive precursors such as agricultural and industrial biomass wastes is highly desirable [4,6]. Various types of biomass have been reported as precursors for activated carbons (AC) production such as garlic peel, corncob, banana peel, rice husk, pine cone, lotus stem, bamboo and nut-shells with CO_2 uptakes in the range of 3–6.5 mmol/g at 1 bar and 0 ºC [8].

AC preparation usually involves two steps: (a) transforming biomass in biochar or hydrochar through carbonization or hydrothermal carbonization, respectively; (b) activation at high temperature, usually between 600 and 900 ºC either physically (by steam, CO_2 or O_2) or chemically (with KOH, K_2CO_3, $ZnCl_2$ or NaOH). Previous studies [9] reported that using a two-step procedure it is possible to obtain AC from biomass with high specific surface area. Usually, if the material is only carbonized a carbon with a low surface area or even non-porous is produced and may not be applicable for CO_2 capture. Among activating agents tested, KOH has been extensively used not only due to its capacity to produce AC with high surface area and a good pore size distribution, but also due to its low environmental pollution, corrosiveness and cost. On the other hand, $ZnCl_2$ has been widely used to produce AC essentially from lignocellulosic and cellulosic precursors. It works as a dampening agent and the movement of volatile substances through $ZnCl_2$ saturated pores is not disrupted and volatile substances can be released from the surface of AC during the activation process. Moreover, chemical activators have dehydrating effect and influence pyrolytic decomposition inhibiting the formation of pore-closing tar [10,11].

Among the existing tree species worldwide, *Pinus radiata* is one of the most widely grown. It is native to the central coast of California, but it has been widely planted around the world, particularly in Spain, New Zealand, Australia, and Chile, and is grown over 4.2 million hectares [12]. Among various materials from industrial or agricultural origin, pine (*Pinus radiata*) sawdust, an abundant and inexpensive industrial bio-waste, can be applied for a lot of applications such as sustainable water remediation, production of activated carbon, oil-water separation and high-performance composites fabrication. Specifically, in previous studies sawdust was revealed as an efficient adsorbent for dyes and heavy metals [10–13]. This residue presents disposal problems and for that reason its recycle and reuse provides a sustainable solution. However, to the best of authors' knowledge, there is a very limited number of studies on CO_2 adsorption applying AC from pine sawdust [14,15] and there are no studies specifically applying the species studied in the present work.

The aim of this study was the synthesis of carbons from pine sawdust to be used as CO_2 adsorbents. A series of ACs were obtained by changing the activation temperature, activating agent and doses of activating agent. The study of the surface and textural characteristics of carbons was performed through different techniques such as scanning and transmission electron microscopy (SEM and TEM), surface area determination by the Brunauer-Emmett-Teller (BET) method, porosity by Barret-Joyner-Halenda (BJH) method and elemental analysis. X-ray diffraction (XRD) was used to analyze the crystalline structure and the surface elemental composition and functional groups by X-ray photoelectron spectroscopy (XPS). The CO_2 adsorption capacity of carbon samples was assessed under different values of gas pressure (0–760 mmHg) at various temperatures 0 ºC, 25 ºC and 50 ºC. Moreover, the experimental equilibrium data for the adsorption under pure CO_2 and N_2 were evaluated by applying the Langmuir, Freundlich and Toth isotherm models. Finally, these data were used for the estimation of the apparent and Ideal Absorbed Solution Theory (IAST) selectivity of CO_2 over N_2.

2. Experimental

2.1. Chemicals

Pine (*Pinus radiata*) sawdust (PS) was provided by a regional sawmill (Lugo, Spain) and received in a bag pre-packed by the supplier. Potassium hydroxide (KOH, 85 %, Probus), zinc chloride ($ZnCl_2$, 98 %, Scharlau), and hydrochloric acid (HCl, 37 %, Sigma Aldrich) were used.

2.2. Carbonization procedure

PS was prepared by air-drying, sieving to a fraction between 0.5 and 1 mm and stored in a plastic container before being used as an organic precursor for the preparation of biochar and activated carbons. Then, to select the optimal carbonization and activation temperatures, the thermal behavior of sawdust was studied by using a thermogravimetric analyzer (TGA Q500, TA Instruments) [16]. One biochar (BC) and five types of activated carbons were synthetized via thermal treatment in a horizontal tubular furnace (Carbolite, Sheffield). PS was carbonized at 600 ºC under inert N_2 atmosphere (10 mL/min) at a heating rate of 5 ºC/min and held for 1 h before cooling to room temperature, and finally was ground in a mortar.

2.3. Activation procedures

The obtained BC was mixed with KOH pellets by a dry procedure at a weight ratio of 1:4 and two different temperatures, 850 ºC and 600 ºC (ACPS850-K-4 and ACPS600-K-4) and at a weight ratio of 1:2 and 850 ºC (ACPS850-K-2). It has been reported that carbon porosity and surface area are affected by the ratio of KOH to biomass and high surface area and porosity were obtained for AC prepared from agricultural biomass using a 1:4 ratio [4]. The samples were placed into the tubular furnace under nitrogen atmosphere (10 mL/min) using a heating rate of 5 ºC/min to reach the selected temperature and, finally, kept for 2 h [17].

Also, another activating agent was employed, $ZnCl_2$, at a weight ratio of 1:4, and the chemical activation was performed both by dry [16] and wet methods at 850 ºC. The $ZnCl_2$ activated carbons were called ACPS850-Z-D and ACPS850-Z-W, respectively. For wet activation, after carbonization a 25 % $ZnCl_2$ solution was mixed with the corresponding biochar mass for 22 h and then dried at 105 ºC for 2 h [18]. For dry activation, the procedure was as previously explained for KOH. In both cases, the activation conditions were as described above.

Finally, after activation, the samples were washed with 100 mL of 0.1 M HCl under stirring for 15 min, then with distilled water under vacuum filtration and dried overnight at 105 ºC [17].

The yield of each carbon was calculated following Eq. (1):

$$Y \quad (\%) = \frac{W_{AC \quad final}}{W_{initial}} \times 100 \tag{1}$$

where Y denotes the yield of biochar or AC obtained after washing, and $W_{initial}$ and $W_{AC\ final}$ correspond to the initial weight of sawdust and final weight of AC on dry basis, respectively.

2.4. Characterization

The morphology of the prepared materials was characterized by scanning electron microscopy on a ZEISS EVO LS 15 microscope and by transmission electron microscopy (TEM). TEM was carried out on a JEOL JEM 2010 transmission electron microscope operated at 200 keV. For TEM measurements, the samples were sonicated in ethanol to form a homogeneous suspension, dropped on a 400 mesh copper TEM grid coated with a thin amorphous carbon film, and then allowed to dry in air.

The specific surface areas were determined by the Brunauer-Emmett-Teller (BET) equation through N_2 adsorption-desorption isotherms at − 196 °C and CO_2 adsorption at 0 °C in a Micromeritics ASAP 2020 sorption analyzer. Prior to measurements, the samples were degassed at 300 °C for 2 h. Total pore volume was determined from the amount of nitrogen adsorbed at a relative pressure (P/P_0) equal to 0.99. To analyze the pore size distribution of carbons the Barret-Joyner-Halenda (BJH) method was applied. The total micropore (< 2 nm) volume was determined by subtracting mesopores (2–50 nm) volume from the total obtained from the adsorption-desorption N_2 isotherm. X-ray diffraction (XRD) was used to analyze the crystalline structure of activated carbons and the measurements were carried out at room temperature in Bragg-Brentano geometry using a BRUKER D8 ADVANCE type X-ray diffractometer (40 kV, 40 mA, theta/theta) equipped with a sealed X-ray tube (CuKα1, λ = 1.5406 Å), and a LYNXEYE XE-T type detector. The diffractograms were obtained in the angular range of $5 < 2\Theta < 60^{o}$ with a step of 0.04° at 4 s per step. The samples were rotated during the measurement to obtain the most optimal peak profile for the analysis, as well as to minimize the effect of the preferred orientation. The BC and activated carbons were analyzed for carbon, nitrogen, hydrogen, sulfur and oxygen (by difference) content using a Flash Smart CHNS Elemental Analyzer (Thermo Scientific). The surface elemental composition and surface functional groups of the materials were determined by X-ray photoelectron spectroscopy (XPS) technique using a Thermo Scientific NEXSA (XPS) instrument equipped with aluminum Kα monochromatized radiation at 1486.6 eV X-ray source. Photoelectrons were collected from a take-off angle of 90° relative to the sample surface. The measurement was done in a Constant Analyser Energy mode (CAE) with a 100 eV pass energy for survey spectra and 20 eV pass energy for high resolution spectra. Charge referencing was done by setting the lower binding energy C1s photo peak at 284.80 eV C1s hydrocarbon peak. Surface elemental composition was determined using the standard Scofield photoemission cross sections.

2.5. CO_2 and N_2 adsorption

The static CO_2 and N_2 adsorption were evaluated using the adsorption isotherms obtained by the volumetric system Micromeritics ASAP 2020 analyzer at the required temperatures (0, 25 and 50 °C) and a pressure range between 0 and 760 mmHg. Prior to experiments, the samples were degassed at 300 °C for 2 h under vacuum to eliminate moisture and impurities. To maintain the targeted temperature, an ice bath in a Dewar was used for experiments at 0 °C and a temperature-controlled vessel using a Selecta Sensoterm sensor for other temperatures.

N_2 and CO_2 adsorption data at different temperatures were fitted to Langmuir (Eq. (2)), Freundlich (Eq. (3)) and Toth (Eq. (4)) models:

Langmuir model:

$$n = \frac{n_{m,L} \cdot K_L \cdot P}{1 + K_L \cdot P} \tag{2}$$

Freundlich model:

$$n = K_F \cdot P^{\frac{1}{n_F}} \tag{3}$$

Toth model:

$$n = \frac{n_{m,T} \cdot K_T \cdot P}{\left\{1 + (K_T \cdot P)^t\right\}^{\frac{1}{t}}} \tag{4}$$

where n (mmol/g) is the loading of adsorbate, P (mmHg) is the pressure and $n_{m,L}$ (mmol/g), $n_{m,T}$ (mmol/g), K_L (1/mmHg), K_F (mmol/g·mmHg$^{1/nF}$), K_T (1/mmHg), n_F and t are the corresponding isotherms' parameters.

The experimental data corresponding to adsorption isotherms of each gas were employed to calculate CO_2 over N_2 apparent and IAST selectivity values. The last one was estimated using GraphIAST software package based on Python module pyIAST [19].

2.6. Statistical analysis

For the activated carbons with $ZnCl_2$, due to the possible similarities, the experiments regarding the specific surface areas were done in quadruplicate and the values averaged. The existence of significant differences among the results for surface areas was analyzed. Thus, the one-way analysis of variance (ANOVA) was used, followed by Brown–Forsythe test according to the significant level. All statistical tests were performed at a 5 % significance level using IBM SPSS Statistics 28 software.

3. Results and discussion

3.1. Effect of experimental parameters on yield

The effect of activating agent, ratio of the carbon to activating agent and activation temperature on the yield was evaluated and the results are presented in Table 1. Carbonization temperature was 600°C for biochar and all activated carbons.

Carbonization essentially involves the pyrolytic decomposition of the precursor and non-carbon species removal [20]. Regarding BC, as expected and observed by the yield percentage, a significant loss of weight was found during the carbonization process as most of the non-carbon elements are released while a carbon skeleton is produced. This result was expected due to a higher mass loss occurred between 200 and 400 °C probably due to cellulose and hemicelluloses decomposition, as well as loss of the leftover adsorbed water. Between 150 and 750 °C lignin decomposition takes place which leads to a less significant decrease on the weight [21,22]. Between 600 and 850 °C there was no mass loss with the increase in the temperature [16]. Similar yields were reported by Tomczyk et al. [23] for biochars produced from wood wastes and sunflower husks.

For the activated carbons, a significant loss in the yield (around 50 %) took place using KOH, while the loss with $ZnCl_2$ was negligible in comparison with BC. This can be due to the fact that during activation with $ZnCl_2$, a polymerization occurs which leads to the creation of a small number of large-ring aromatic compounds. Likewise, $ZnCl_2$ inhibits the volatile matter loss, stabilizing it and eventually increasing the yield in comparison with KOH which typically produces yield losses between 10 % and 40 % [20,24]. However, KOH has been extensively used, as AC with high surface area and porosity is produced due to cavity formation by KOH evaporation from places previously occupied by it. Probably, this fact is due to a mechanism in which the alkali metal interposes in the carbon matrix acting as an electron donor that ignites the reaction during gasification. Also, the presence of oxygen could remove the carbon atoms cross-linking in the crystallites. The release of

Table 1
Effect of experimental parameters on yield of carbon samples.

Type of carbon	Activating agent	Carbon to activating agent ratio	Activation temperature (°C)	Yield (%)
BC	-	-	-	20.1 ± 1.1
ACPS850-K-4	KOH	1:4	850	10.1 ± 1.1
ACPS600-K-4	KOH	1:4	600	14.6 ± 1.2
ACPS850-K-2	KOH	1:2	850	12.4 ± 0.6
ACPS850-Z-D	$ZnCl_2$	1:4	850	19.3 ± 1.3 [16]
ACPS850-Z-W	$ZnCl_2$	1:4	850	17.2 ± 1.5

potassium at elevated temperature interposes and forces a part of the separate lamellae of the crystallite. Moreover, the use of this chemical has advantages such as lower environmental pollution, less corrosiveness and lower cost [20,24].

Additionally, it can be observed that activation temperature strongly influenced yield with KOH activation since when temperature was reduced from 850 to 600 ºC the yield increased. On the other hand, the effect of the biochar/activating agent ratio on yield was less significant. The influence of these variables on the yield of carbons prepared from sawdust was also reported in literature [25]. As a comparison, Table 2 illustrates results obtained in previous investigations for activated carbons prepared from various agricultural and industrial biomass wastes activated with KOH and $ZnCl_2$ with some similar values to the obtained in this work.

3.2. Structural characterization

To have a comprehensive characterization of the structure and qualitatively analyze the morphology of the prepared carbons SEM analysis was performed. Fig. 1 illustrates the SEM images of biochar and activated carbons derived from pine sawdust. SEM revealed that the biochar and activated carbons particles have a honey-comb structure and an arrangement of uniform holes distributed around the surface typically from lignocellulosic materials [32,33].

The carbonized pine sawdust (Fig. 1a) presented few pores in the walls, and this can be ascribed to the decomposition of the pine sawdust natural compounds, such as cellulose, hemicellulose and lignin, during the carbonization process. This initial porosity can facilitate the activating agents access into the carbonized material. After activation with KOH and $ZnCl_2$ the carbonized material maintained the structure, however, the carbon activated with KOH at highest ratio (Figs. 1b and 1c) showed more modifications in the structure which can be due to the strong activation under these conditions. The rupture caused by this agent could explain the obtention of a high specific surface area for these carbons. For carbons with $ZnCl_2$ activation the presence of pores is less evident (Fig. 1e and f) due to the high percentage of microporosity, as will be seen later, that plays a fundamental role in CO_2 adsorption [6].

Furthermore, TEM analysis was implemented to disclose the morphology of the carbons since can provide more information about micropores. The results are illustrated by Fig. 2.

It is possible to observe an abundant disorderly wormhole-like micropore structure on the surface of the materials, which is due to the stacking of graphene layers and indicates a significant amount of microporosity as supported by the textural characterization by N_2 adsorption isotherms. The randomly distributed micropores throughout the carbon skeleton without any pattern indicate the amorphous feature of these adsorbents as inferred by the XRD results (Fig. 3). Besides, the results show that a morphological improvement occurred after the activation process both with KOH or $ZnCl_2$ in agreement with SEM analysis.

Table 2
Comparison of yield of activated carbon prepared from various agricultural wastes and an industrial by-product (Slash pine wood) using $ZnCl_2$ and KOH.

Precursor	Activating agent	Carbon to activating agent ratio (w/w)	Activation temperature (ºC)	Yield (%)	References
Safflower biochar	$ZnCl_2$	1:4	900	26.0	[26]
Waste potato residue	$ZnCl_2$	1:1.5	600	29.2	[27]
Vine shoots	$ZnCl_2$	1:1.3	700	18.2	[28]
Cane pith	KOH	1:5	780	8.2	[29]
Rice straw	KOH	1:4	800	13.5	[30]
Maize stalks	KOH	1:0.75	700	13.1	[31]
Slash pine wood	KOH	1:4	580	24.5[a]	[18]
Slash pine wood	$ZnCl_2$	1:1	580	26.8[a]	[18]

[a] Normalized yield calculated from biochar.

As above mentioned, the crystallographic structure of BC and activated carbons was evaluated from the XRD data, which is shown in Fig. 3. As can be seen, the materials show different degrees of graphitization. The samples activated at higher temperature (850 ºC) with KOH as activated agent show a similar behavior practically without peaks in the diffractograms, while the other ones presented broad diffraction peaks at different ranges (Table 3).

In this way, the weak broad peaks in ACPS850-K-4 and ACPS850-K-2 indicate that these carbons have an amorphous structure with a very low graphitization degree [8]. The other materials show a different degree of amorphous behavior with broad peaks at similar ranges, except for BC. The weak and broad peaks at 2Θ values of around 23º and 43º correspond to the (002) and (100) diffraction of graphite carbon, respectively. Their weak intensities indicate a low crystallinity degree or a partially graphitic crystal structure. The fact that the X-ray diffraction spectrum did not show well-defined peaks, in any case, indicates that no discrete mineral phase was detected. The humps in the 2Θ range (Table 3) are related to the high degree of disorder of carbonaceous materials [34,35]. Thus, ACPS600-K-4 presented the highest graphitization order while the lowest one corresponds to ACPS850-K-4. A possible explanation can be that the activation with KOH at high temperature destroys the atomic arrangement of the samples, as the increase in porosity demonstrates. Concerning the different behavior for the BC, previous studies reported that the microcrystalline structure in biochars can be created due to the superposition of multiple aromatic layers. The diffraction peak at 23.2º characterizes the degree of spatial parallelization and azimuthal orientation of the aromatic layer in the microcrystalline structure. Similar results were reported by Quan et al. [14] for a biochar produced from pine sawdust at 700 ºC. Moreover, the high and narrow peak indicates a better orientation. Additionally, the diffraction peak (100) depicts the size of the aromatic layer. If the peak is high and narrow, this indicates that the diameter of the aromatic layer is large, which means that the degree of aromatic nuclear polymerization is high [14]. As can be observed by Fig. 3 all materials revealed a marked peak at 43º (100), except the carbons activated with KOH at 850 ºC.

Elemental analysis was also performed, and the results are listed in Table 4. The high carbon content determines the highly carbonaceous nature of the adsorbents, that is an important factor to produce high porosity and hence high CO_2 uptake [36]. ACPS850-K-4 is the sample with the highest carbon content (90.3 %), which may enhance the inter-particle force between the CO_2 molecules and the adsorbent [37].

It seems that after KOH activation at higher temperature, independently of KOH ratio used, the hydrogen content decreased since BC goes through dehydrogenation and intermolecular dehydration during activation process. On the contrary, at lower temperature (600 ºC) the hydrogen content increased. The content of hydrogen also decreased after activation with $ZnCl_2$, as expected due to dehydrogenation, but it was less significant [24]. The content of nitrogen was maintained except for the carbon activated with $ZnCl_2$ by the dry method in which it increased, possibly due to a changes in the nitrogen functional groups.

Oxygen content varied from 9.4 % to 46.2 % which can explain a different behavior of carbons on the CO_2 adsorption, although really the effect of oxygen is controversial since some studies reported that the surface oxygen complexes influence CO_2 adsorption, but others showed that oxygen heteroatoms in hydroxyl and carboxyl functional groups may enhance CO_2 uptake [37]. The high oxygen content for ACPS600-K-4 may be attributed to gasification reactions and formation of oxygen groups during activation process at lower temperature in the presence of KOH, which in the present study possibly enhanced CO_2 uptake. At high temperature more decomposition reactions occur which

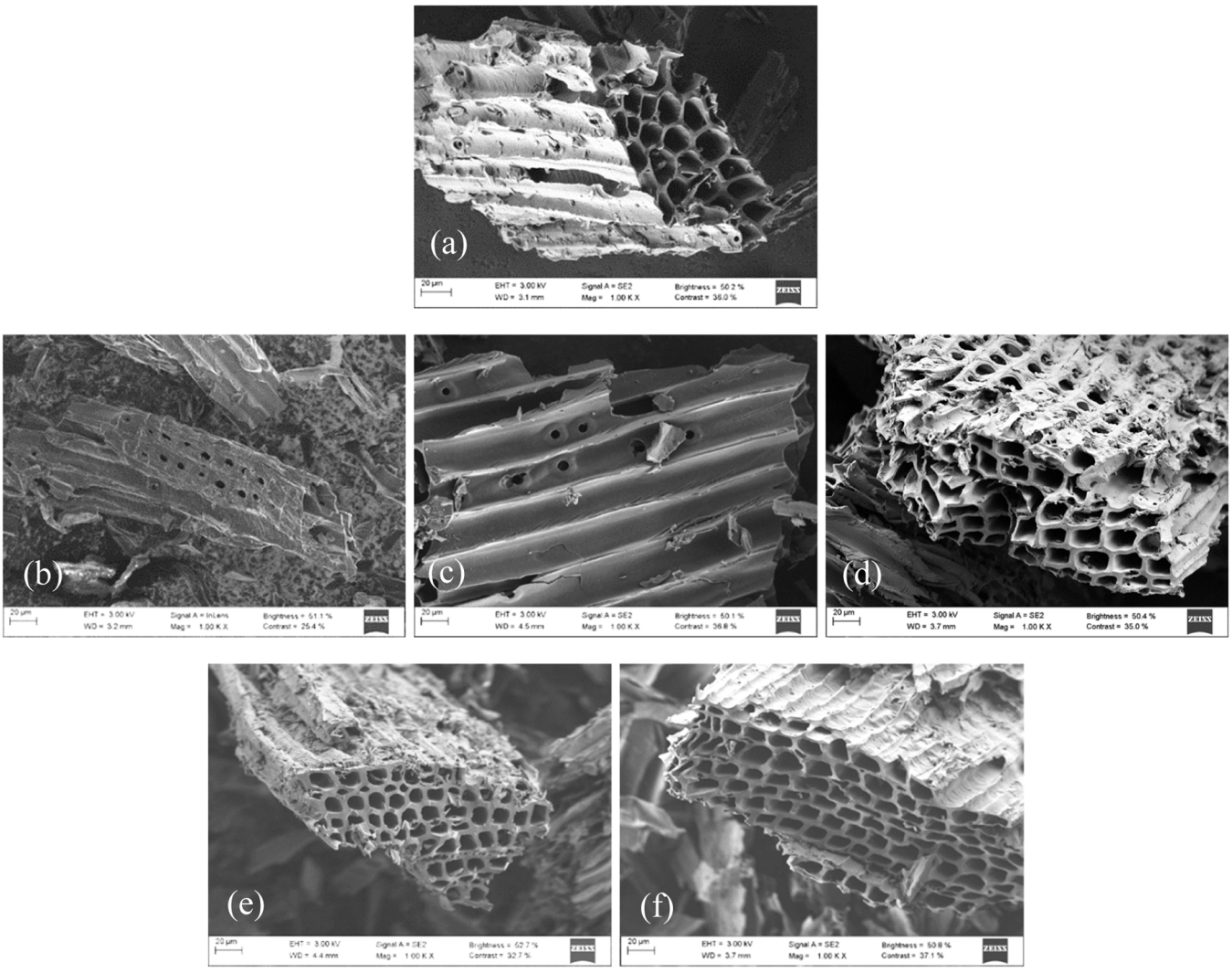

Fig. 1. SEM images of (a) BC, (b) ACPS850-K-4, (c) ACPS600-K-4, (d) ACPS850-K-2, (e) ACPS850-Z-D and (f) ACPS850-Z-W.

can lead to a decrease in oxygen content [38]. The decrease in oxygen content for the carbons activated with $ZnCl_2$ could be due to the catalytic dehydration caused by $ZnCl_2$ [39].

Moreover, as seen in Table 4, for KOH activated carbons, hydrogen and oxygen content decreased with increasing the activation temperature to 850 °C. Also, an increase in aromaticity for these activated carbons was observed due to the H/C ratio decrease, although for ACPS850-K-4 and ACPS850-K-2 the H/C ratio was very similar. Activation with $ZnCl_2$ produced changes respect to BC reducing the H/C ratio but in less proportion than KOH. On the other hand, the H/C ratio decreased as a result of activation, except for ACPS600-K-4, which showed the highest H/C and O/C ratios indicating a low degree of carbonization and aromaticity and a high polarity [40,41].

In addition, wide XPS spectra analysis has allowed to determine the elemental composition of the carbons' surface and the results are presented in Fig. S1 and Table 5. As seen previously, C and O are the two main components as confirmed by the O1s and C1s peaks (Fig. S1) appearing at 285–287 and 532.5 eV, respectively. A weak feature around 400 eV belongs to N1s photoelectrons, revealing a very low atomic percentage (at%) of nitrogen in almost all samples. These results were consistent with the elemental analysis results (Table 4). Other elements were detected such as silicon, potassium, chlorine, calcium, and sulfur, all in very low concentrations. Traces of inorganic fractions (i.e., Si, Ca…) detected in XPS analysis can come from ashes or from the activated carbon precursors [42].

To obtain further insight on the type of bonding of these elements high resolution spectra for C1s, N1s and O1s were analyzed, and the results are shown in Table 6.

Five peaks were observed in the C1s high resolution spectra and four contributions per carbon. The most abundant contribution was that at 284.8 eV that is usually assigned to C-C, C═C or C-H bonds. In addition, in the C1s spectrum of the sample ACPS600-K-4, the K2p3/2 and K2p1/2 contributions from the spin-orbit splitting of the 2p orbital was clearly observed (Fig. S2) and can be attributed to potassium cations and oxides which means that probably potassium ions bind to remaining oxygen atoms or are intercalated within carbon [43]. On the other hand, the carbons activated with KOH at high temperature had a lower C-C content which can be due to the interaction between KOH and carbon that caused partial degradation of graphite layer destroying the matrix structure [14]. These results are in agreement with XRD results in which ACPS850-K-4 and ACPS850-K-2 presented a very low degree of graphitization. Regarding N1s high resolution spectra, they were fitted with only one component, pyrrolic-N, except for ACPS850-K-4. According to previous studies [44], pyrrole/pyridine-N group can contribute to CO_2 adsorption due to its strong interaction with CO_2 molecules. The O1s high resolution spectra were fitted with two, three or four components depending on the carbon. The binding energy peaks between 532.6 and 533 eV can be assigned to non-carboxyl oxygen (ether structures) in esters and anhydrides and those between 533.1 and 534.0 to oxygen atoms in carboxyl groups (-COOH and –COOR) [45]. The most abundant

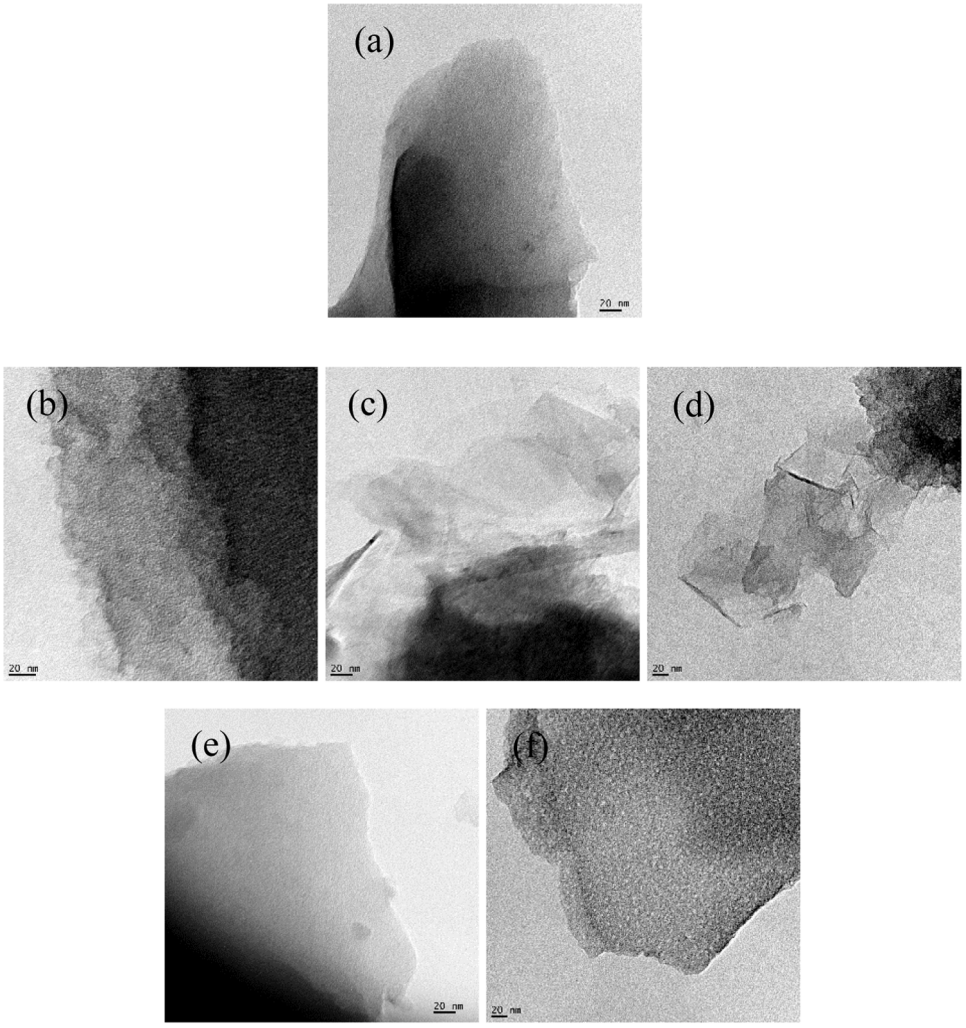

Fig. 2. TEM images of (a) BC, (b) ACPS850-K-4, (c) ACPS600-K-4, (d) ACPS850-K-2, (e) ACPS850-Z-D and (f) ACPS850-Z-W.

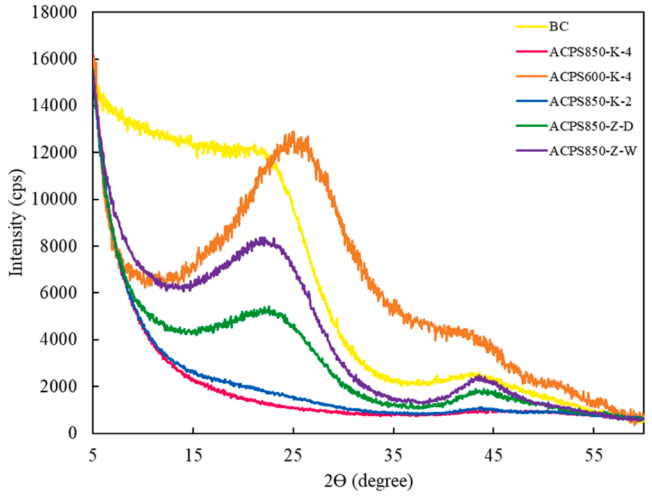

Fig. 3. XRD diffractograms of biochar and activated carbons.

peak was that at 532.6–533 eV for most carbons, but it was not detected for those activated with KOH at the highest ratio. XPS analysis demonstrated the presence of various functional groups in the carbons that suggest that although physical adsorption can be dominant as revealed the CO_2/N_2 selectivity and the isosteric heat of adsorption (see Sections

Table 3
Diffraction peaks of biochar and activated carbons.

Material	2Θ (degree)				
BC	16.8	23.2	42.9	49.5	
ACPS850-K-4	44.2	50.2			
ACPS600-K-4	16.8	25.1	42.3	52.1	55.9
ACPS850-K-2	22.8	43.7	48.8		
ACPS850-Z-D	17.6	23.2	43.7	49.0	
ACPS850-Z-W	18.2	23.4	43.7	49.5	

Table 4
CHNS elemental analysis of BC and activated carbons.

Sample	Elemental analysis (wt%)					
	C	H	N	O*	H/C	O/C
BC	83.71	2.40	0.14	13.75	0.029	0.16
ACPS850-K-4	90.27	0.17	0.081	9.48	0.0022	0.10
ACPS600-K-4	50.61	3.12	0.13	46.14	0.061	0.91
ACPS850-K-2	88.02	0.20	0.14	11.64	0.0022	0.13
ACPS850-Z-D	80.05	1.18	0.38	18.39	0.015	0.23
ACPS850-Z-W	84.05	0.97	0.14	14.84	0.012	0.18

* by difference

Table 5
Elemental composition of the carbons' surface by XPS analysis.

Material	Elemental composition (at%)							
	C	O	N	Si	Ca	K	Cl	S
BC	88.65	9.29	0.47	0.91	0.68	-	-	-
ACPS850-K-4	91.62	6.07	-	1.10	0.48	0.49	0.23	-
ACPS600-K-4	79.99	16.51	1.08	0.94	-	1.20	0.28	-
ACPS850-K-2	88.93	8.44	0.58	1.25	0.80	-	-	-
ACPS850-Z-D	93.10	4.22	1.56	0.57	-	-	0.30	0.25
ACPS850-Z-W	94.86	3.82	0.59	0.59	-	-	0.14	-

3.4.4 and 3.5), chemical adsorption can co-exist in the CO_2 separation process [44].

3.3. Specific surface area and porosity

To assess the surface area and porosity of the synthesized materials this study recorded gas sorption-desorption N_2 isotherms at − 196 ºC (Fig. 4) and pore size distribution (Fig. 5).

The N_2 isotherms of all carbons are essentially reversible Type I isotherms, according to the IUPAC classification that agrees with some previous studies using biomass as raw material [9,35]. The sharp uptake at low relative pressure ($P/P_0 < 0.1$) suggests that the synthetized materials are fundamentally microporous with pores highly accessible to the gas molecules and maybe with small mesopores [1]. When the amount adsorbed reaches the limited uptake a monolayer is formed with strong adsorbent-adsorbate interactions in the narrow micropores. Type I isotherms can be subdivided in isotherm type I (a) and type I (b). From Fig. 4 it is possible to conclude that ACPS850-K-4, ACPS850-K-2 and ACPS600-K-4 present type I (b) isotherms which characterize materials with a pore size distribution of wider micropores and narrow mesopores (< 2.5 nm). In this case, a slight curvature is present in Fig. 4 which implies a wide relative pressure range in which the presence of a knee can be observed. This behavior implies that apart from the monolayer formed before reaching the highest value of nitrogen adsorption, a multilayer formation occurs. This is usually observed for large micropores size that allow multilayer formation into the pores. However, the BC and the carbons activated with $ZnCl_2$ (ACPS850-Z-D and ACPS850-Z-W) show type I (a) isotherm corresponding to microporous materials with primarily narrow micropores (< 1 nm) [46]. On the other hand, the amount of adsorbed nitrogen reveals that biochar activated with KOH substantially develops its morphology.

Indeed, Fig. 5 indicates that for all the carbons the amount of pores with size higher than 10 nm is negligible. For those activated with KOH, the volume of available pores in the porous structure increases significantly with small changes in their size, mainly for pore diameters lower than 7 nm. Particularly, for that activated at 850 ºC with a KOH ratio of 1:4 (w/w) pores with higher size were detected which is in agreement with its lower microporosity percentage. The behavior is different for the BC and the carbons activated with $ZnCl_2$ in which both pore volume and size were lower. In general, the pore size distribution indicates that the porosity of the materials consists mainly of micropores and a few mesopores.

The textural parameters of the prepared adsorbents calculated from N_2 adsorption isotherms at − 196 ºC and CO_2 adsorption isotherms at 0 ºC are shown in Table 7.

Previous results confirm the activation process efficiency since BET surface area and pore volume increased significantly for all activated carbons. The activating agent is directly related to the specific surface area of the material, determined with N_2 adsorption, as for the ones activated with KOH the specific surface area is considerably superior to that of those activated with $ZnCl_2$. For instance, ACPS850-K-4 has a surface area 83.5 % and 80.9 % higher than those of ACPS850-Z-D and ACPS850-Z-W, respectively. This evidence confirms the results shown in the SEM images which revealed that activation with KOH caused major

Table 6
Components and relative proportions for C1s, N1s and O1s.

Material	C1s (%)					N1s (%)	O1s (%)			
	C-C, C=C, CH_x (284.8 eV)	C-O-C, C-OH (286.1–286.5 eV)	C=O (288–288.3 eV)	O=C-O (289 eV)	CO_3 (290.3 eV)	Pyrrolic-N (399.9–400.8 eV)	OH groups (531–531.8 eV)	Organic bonds (532.6–533.0 eV)	Organic bonds (533.1–534.0 eV)	$H_2O_{adsorbed}$ (534.3–535.4 eV)
BC	70.60	22.31	4.69	2.39	-	100	22.02	39.94	32.48	5.57
ACPS850-K-4	62.47	19.28	10.25	-	8.01	-	56.44	-	43.56	-
ACPS600-K-4	70.70	15.10	11.04	-	3.17	100	41.26	-	54.34	4.39
ACPS850-K-2	67.01	17.80	10.18	-	5.00	100	37.41	49.13	-	13.46
ACPS850-Z-D	73.90	18.08	4.67	-	3.35	100	12.48	69.77	-	17.74
ACPS850-Z-W	77.94	13.74	5.14	-	3.18	100	20–73	60.63	18.64	-

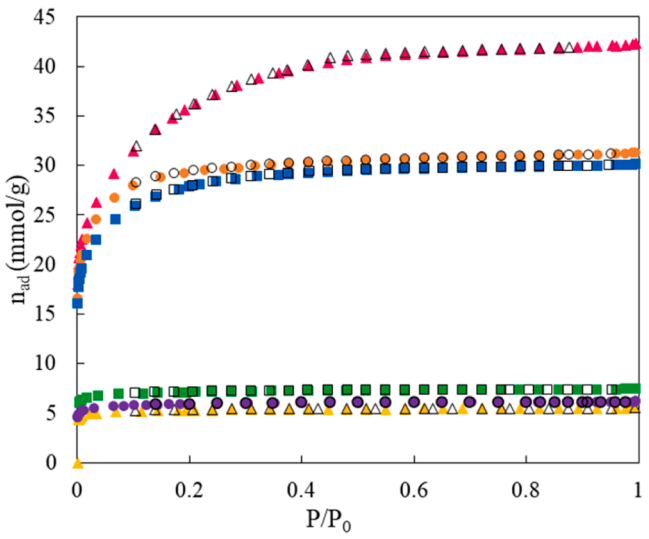

Fig. 4. Nitrogen adsorption/desorption isotherms at − 196ºC. ▲ and Δ: BC; ▲ and Δ: ACPS850-K-4; ● and ○: ACPS600-K-4; ■ and □: ACPS850-K-2; ■ and □: ACPS850-Z-D; ● and ○: ACPS850-Z-W. Full symbols: adsorption. Empty symbols: desorption.

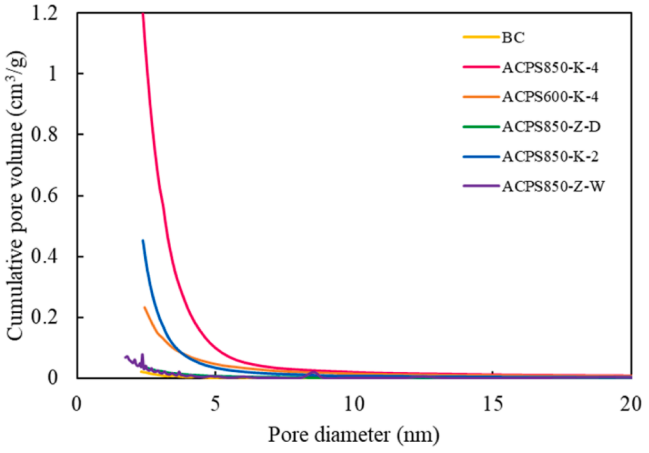

Fig. 5. Pore size distributions for biochar and activated carbons.

changes in the structure and consequently surface area and porosity increased.

Regarding the carbons activated with KOH, it can be observed that an increase in the activation temperature from 600 to 850ºC increased the specific surface area determined with N_2 adsorption by around 17%. On the other hand, the rise in the activating agent mass ratio from 1:2–1:4 (w/w) increased the surface area by around 26%. These results show that both activation temperature and activating agent mass ratio are important process parameters influencing the magnitude of the surface area. On the other hand, in all carbons activated with KOH the surface area calculated with N_2 adsorption was higher than 2000 m^2/g, however, the highest surface area calculated with CO_2 was for ACPS600-K-4 with the highest CO_2 uptake followed by ACPS850-K-4. Nevertheless, ACPS850-K-2 with low surface area showed higher CO_2 uptake, revealing the importance of micropore presence. Therefore, the mild experimental conditions (ACPS600-K-4 and ACPS850-K-2) are better for CO_2 adsorption than extreme conditions. Concerning $ZnCl_2$, the difference for the specific surface area determined with N_2 of the carbons prepared by both activation methods was lower than 7%, therefore the dry method was the one selected for being a more environmentally friendly option.

The total pore volume was higher for the KOH activation, mostly for the one activated with the highest BC/KOH ratio which confirms that a higher ratio favors the formation of pores with higher diameters, which is also in agreement with the surface area values [9]. Another interesting finding is that the use of $ZnCl_2$ (mainly for dry activation) leads to an increase in the N_2 and CO_2 surface areas maintaining the microporosity percentage in comparison with BC, which is very important since several research stand out the importance of small micropores for CO_2 adsorption [2,6,47]. CO_2 uptake is more closely related to the micropore volume rather than to surface area since the minimum uptake occurred for ACPS850-K-4 with the lowest microporosity percentage and the highest surface area.

To obtain a greater insight regarding the porosity of the carbons produced, CO_2 adsorption isotherms at 0 ºC were used to provide a good estimation of surface area provided by the carbon ultra-microporosity (lower than 0.7 nm) [9,48]. Fig. 6 shows the CO_2 adsorption isotherms of the carbon samples prepared. The experimental data show a monotonic increase in the adsorbed amount of gas without reaching a *plateau* due to the low relative pressure values employed in this characterization technique.

Interestingly, the adsorption isotherms indicate that for P/P_0 values above 0.01, BC exhibits the lowest CO_2 uptake and the carbons activated with KOH the highest ones, with distinction for ACPS600-K-4 that presented the highest value reaching 5.8 mmol/g at 0.03. Such differences can be related to their BET surface areas (with N_2 and CO_2) and microporosity. On the other hand, a different behavior is observed for pressure values below 0.01, at which ACPS600-K-4 is still maintaining the highest CO_2 uptake but without considerable differences among all carbons. Furthermore, BC reaches a higher CO_2 uptake than the activated carbons. This can be due to the key role of ultra-micropores in the CO_2 adsorption at low partial pressures as previously stated by Hao et al. [7]. Moreover, at 0 ºC CO_2 adsorption occurs via the pore filling mechanism being critical the pore size [2]. Apart from that, since BC is only carbonized at 600 ºC some functional groups based on lignin fraction that can participate in CO_2 adsorption were better preserved [49].

Table 7
Textural characterization by N_2 adsorption isotherms at − 196ºC and CO_2 adsorption isotherms at 0ºC.

Sample	Adsorption Isotherm N_2 at − 196 ºC					Adsorption Isotherm CO_2 at 0ºC	
	S_{BET} (m^2/g)	Total Pore Volume (cm^3/g)	Mesopore Volume (cm^3/g)	Micropore Volume (cm^3/g)	Microporosity (%)	S_{BET} (m^2/g)	CO_2 uptake[1] (mmol/g)
BC	293.3 ± 7.7	0.19	0.02	0.18	90.7	254.8 ± 1.3	1.17 ± 0.12
ACPS850-K-4	2864.5 ± 0.9	1.46	0.47	0.99	67.8	677.2 ± 0.2	1.03 ± 0.16
ACPS600-K-4	2437.2 ± 5.6	1.09	0.12	0.97	89.0	1354.2 ± 21.8	1.65 ± 0.21
ACPS850-K-2	2270.5 ± 22.5	1.02	0.15	0.87	85.0	588.1 ± 25.9	1.33 ± 0.19
ACPS850-Z-D*	471.4 ± 18.4[a]	0.26	0.02	0.23	90.6	319.5 ± 3.9[a]	1.41 ± 0.15
ACPS850-Z-W	501.1 ± 41.6[a]	0.26	0.03	0.23	88.9	382.1 ± 34.6[a]	1.56 ± 0.15

[1]determined at 105 mmHg; CO_2/N_2 mixture (15 % volume CO_2)
* [16]
[a] different letters indicate significant differences ($p \leq 0.05$) between samples

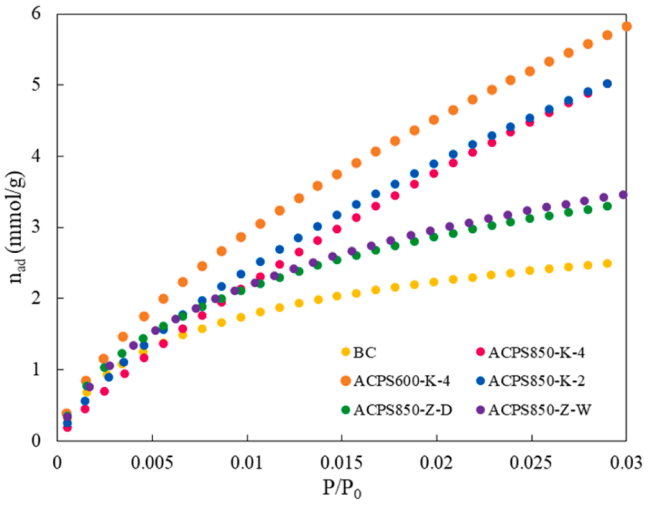

Fig. 6. CO_2 adsorption isotherms at 0ºC for BC and AC prepared.

On the other hand, CO_2 uptake was higher for those AC with higher microporosity percentage (ACPS600-K-4, ACPS850-Z-D and ACPS850-Z-W) as shown in Table 7.

3.4. Adsorption experiments

3.4.1. N_2 and CO_2 adsorption isotherms at 25 ºC

The N_2 and CO_2 adsorption capacities of the carbons prepared from pine sawdust were examined. Fig. 7 presents the N_2 and CO_2 adsorption isotherms of samples at 25 ºC. All carbons presented greater adsorption capacity for CO_2 than for N_2 over the entire pressure range. Besides, CO_2 adsorption isotherms can be classified as Type I which are typical of stronger adsorbate-adsorbent interactions [47].

Regarding N_2 adsorption, there are no substantial differences at low pressures despite differences among surface areas (Table 7). On the contrary, in the range of high pressures, other aspects such as chemical interactions or adsorption kinetics can influence and, thus, some slight differences in N_2 adsorption capacity among carbons were found [9].

Regarding CO_2 adsorption, particularly for the low-pressure region, the BC adsorption capacity is similar to that of the activated carbons due to the preservation of the chemical surface and the importance of the microporosity. On the other hand, for the high-pressure region the smaller CO_2 uptake on BC is due to its low surface area and probably to micropore filling. Although ACPS850-K-4 presented the highest surface area had lower CO_2 uptake than the carbons activated with KOH at lower temperature and BC/KOH ratio. Thus, ACPS600-K-4 showed the largest CO_2 uptake (3.59 mmol/g) which can be related not only to its high CO_2 BET surface area generated by the ultramicroporosity, but also to its high microporosity which largely favors CO_2 capture [1]. These results are also in agreement with elemental analysis and XPS in which the high oxygen content can favor the CO_2 uptake (Table 4). Conversely, in the low-pressure region the trend is not the same, since ACPS600-K-4 showed the best results followed by the carbons activated with $ZnCl_2$. This can be explained considering that at low pressures the presence of ultra-micropores is responsible for most of CO_2 uptake and these carbons presented the higher microporosity percentages (Table 7) [9]. Additionally, as $ZnCl_2$ activation is less aggressive, surface changes are minor which allows a higher affinity between adsorbent and adsorbate. In general, it is possible to infer that a large surface area (mainly due to low-size pores) and high micropore volume are mandatory requirements in CO_2 uptake as stated in previous investigations [8].

Thus, since all carbons presented higher uptake for CO_2 than for N_2 this makes them possible candidates in separation/purification of gaseous streams.

3.4.2. Influence of temperature on CO_2 and N_2 adsorption

CO_2 adsorption isotherms at three different temperatures (0 ºC, 25 ºC and 50 ºC) were also collected to study in detail the dependence of CO_2 adsorption on temperature. Fig. 8 displays the adsorbed amount of CO_2 as a function of both temperature and pressure for all carbons prepared.

It is observed that all materials present the same tendency, thereby the amount of CO_2 adsorbed decreases with increasing temperature which is in agreement with previous studies [6,47]. This behavior indicates that the capture of CO_2 by the carbons is a physisorption process [8].

As previously mentioned, for the low-pressure region the carbons activated with $ZnCl_2$ and ACPS600-K-4 presented higher amounts of CO_2 adsorbed which could be indicative of a higher affinity for the material and evidence the influence of the ultra-microporosity on the CO_2 capture. Also, other authors mentioned that the ultra-micropores responsible for CO_2 adsorption are dependent on the adsorption temperature. For instance, at 75 ºC they found that only the ultra-micropores in the range of 0.33–0.40 nm were effective [6,9] which can explain the worst behavior with increasing temperature in this work.

Regarding N_2 adsorption, the same behavior with respect to the

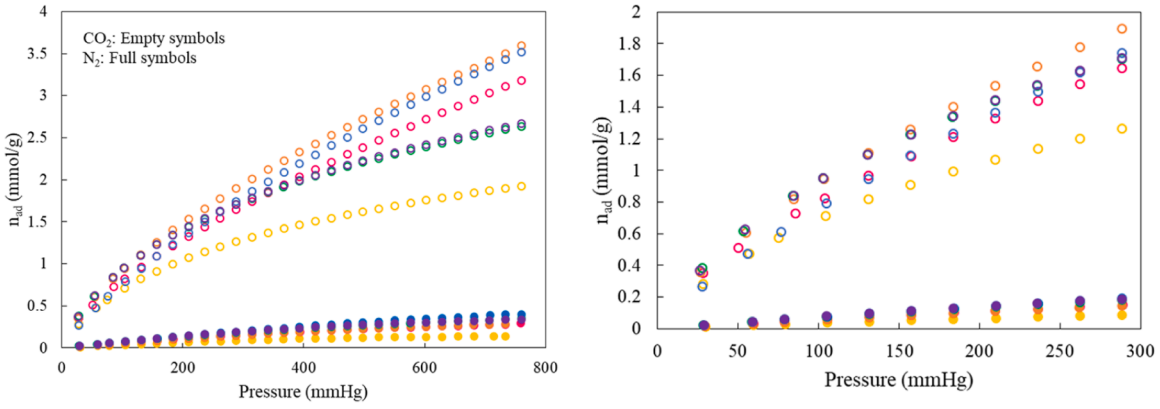

Fig. 7. N_2 and CO_2 adsorption isotherms at 25ºC (right plot is a zoom at the low-pressure range). ● and ○: BC; ● and ○: ACPS850-K-4; ● and ○: ACPS600-K-4; ● and ○: ACPS850-K-2; ● and ○: ACPS850-Z-D; ● and ○: ACPS850-Z-W.

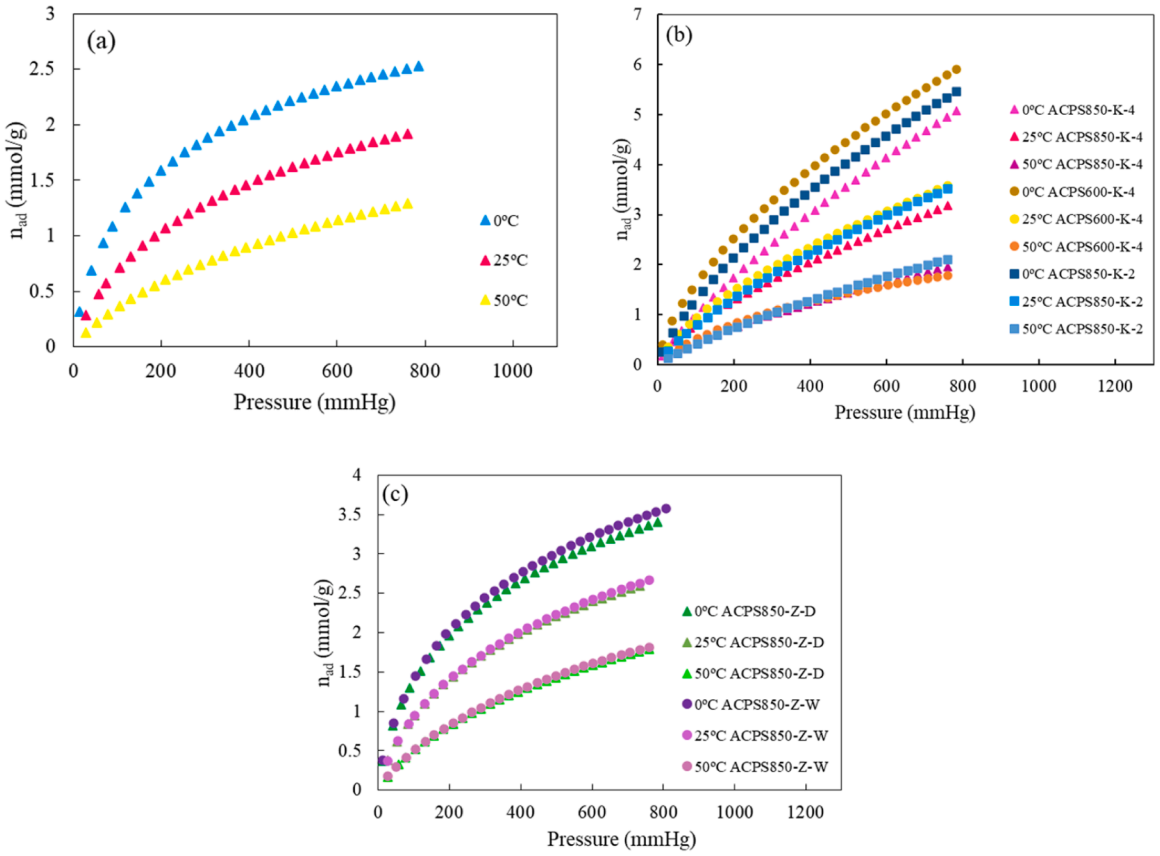

Fig. 8. Adsorption isotherms of CO_2 at different temperature (0 ºC, 25 ºC and 50 ºC) for BC (a) and AC with KOH (b) and $ZnCl_2$ (c).

influence of temperature was observed as for CO_2 adsorption, i.e., a decrease in the amount adsorbed with increasing temperature, being the decrease of N_2 adsorbed more remarkable than for CO_2.

Table 8 lists the CO_2 adsorption capacity of different materials reported in literature. It is noticeable that the pine sawdust derived activated carbon prepared in this study presented a high CO_2 uptake.

Table 8
CO_2 adsorption capacity of different materials reported in literature.

Precursor/ Material	BET Surface area (m^2/g)	Adsorption capacity (mmol/g)	T (ºC)	P (bar)	Reference
Pine nut shell	459–2207	7.7–5.0	0/ 25	1	[6]
Pine nut shell	459–2207	3.3–2.0	0/ 25	0.15	[6]
Pine cone shells	1246–3931	7.6–2.0	0/ 25/ 45	1	[50]
Pine cone shells	1246–3931	2.4–0.6	0/ 25/ 45	0.15	[50]
Water chestnut shell	864–2421	4.5–6.9	25/ 0	1	[51]
Potassium bitartrate	557–1217	3.6–5.2	25/ 0	1	[52]
Petroleum coke	1278	4.2–5.6	25/ 0	1	[53]
Commercial melamine formaldehyde resin	1658	5.0–3.3	0/ 25	1	[54]
Pine sawdust	293–2437	5.8–2.5	0/ 25/ 50	1	This work

Usually, CO_2 adsorption capacity on activated carbons is closely related to their precursors and activating agents. Sawdust is favorable for the preparation of activated carbons since its ordered hollow channels formed after carbonization facilitate the activating agent impregnation and penetration on the pore walls [6].

3.4.3. *N_2 and CO_2 adsorption isotherms at different temperatures*

To better understand and obtain information about the carbon surface properties and their affinity towards both gases, carbon dioxide and nitrogen adsorption experimental data at 0, 25 and 50 ºC were fitted to Langmuir (Eq. (2)), Freundlich (Eq. (3)) and Toth (Eq. (4)) models by means of the Solver tool of Microsoft Excel [55]. Error Sum of Squares (ESS) was employed to assess the performance of the models [1].

Table 9 lists the isotherms parameters for CO_2 adsorption for all carbons at different temperatures and the respective error sum of squares (ESS). Fig. 9 demonstrates, as an example, how the experimental data corresponding to CO_2 adsorption on BC and ACPS850-K-2 fit to Langmuir, Freundlich and Toth models. Toth isotherm best fitted the experimental data for both materials over the entire pressure range for all carbon samples as demonstrate the low ESS values. This model allows to describe the degree of heterogeneity of the multilayer adsorption process.

The t parameter is related to the degree of surface heterogeneity and t values tending to 1 mean that the surface is homogeneous. If t is equal to 1 the Toth model reduces to Langmuir isotherm and if t deviates from 1, the gas-solid system is energetically heterogeneous [9,56]. In this case, t values are between 0.40 and 0.66, therefore, it can be assumed that the surface of all carbons is heterogeneous [1]. In general, an increase in temperature causes a decrease in the adsorption capacity.

Previous investigations suggested that Freundlich model may not be used to describe pure CO_2 adsorption since at high pressures the model cannot explain the sorption behavior [57]. This can be observed in Fig. 9

Table 9
Isotherms parameters for CO_2 adsorption.

	Langmuir			Freundlich			Toth			
T	$n_{m,L}$	K_L	ESS_L	n_F	K_F	ESS_F	$n_{m,T}$	K_T	t	ESS_T
BC										
0	2.99	$6.11{\cdot}10^{-3}$	0.069	2.16	0.127	0.038	4.47	$8.95{\cdot}10^{-3}$	0.53	$1.83{\cdot}10^{-4}$
25	2.56	$3.57{\cdot}10^{-3}$	0.025	1.82	0.053	0.098	4.61	$3.56{\cdot}10^{-3}$	0.53	$1.45{\cdot}10^{-6}$
50	2.09	$2.00{\cdot}10^{-3}$	$7.1{\cdot}10^{-3}$	1.47	0.015	0.035	3.85	$1.40{\cdot}10^{-3}$	0.61	$1.22{\cdot}10^{-4}$
ACPS850-K-4										
0	11.66	$9.17{\cdot}10^{-4}$	0.24	1.23	0.023	0.063	34.69	$3.21{\cdot}10^{-4}$	0.63	0.023
25	5.33	$1.69{\cdot}10^{-3}$	0.22	1.49	0.037	$1.79{\cdot}10^{-3}$	35.27	$4.15{\cdot}10^{-3}$	0.39	0.027
50	3.72	$1.31{\cdot}10^{-3}$	0.062	1.37	0.016	$1.47{\cdot}10^{-4}$	28.53	$2.45{\cdot}10^{-4}$	0.41	$5.97{\cdot}10^{-3}$
ACPS600-K-4										
0	8.86	$2.18{\cdot}10^{-3}$	0.91	1.55	0.082	0.040	20.39	$1.15{\cdot}10^{-3}$	0.57	0.16
25	5.98	$1.74{\cdot}10^{-3}$	0.20	1.47	0.039	0.013	17.34	$7.77{\cdot}10^{-4}$	0.53	0.032
50	4.26	$1.28{\cdot}10^{-3}$	0.057	1.34	0.016	$8.07{\cdot}10^{-3}$	13.63	$4.68{\cdot}10^{-4}$	0.56	$9.11{\cdot}10^{-3}$
ACPS850-K-2										
0	9.64	$1.51{\cdot}10^{-3}$	0.37	1.36	0.042	0.21	42.11	$4.77{\cdot}10^{-4}$	0.46	0.014
25	7.34	$1.13{\cdot}10^{-3}$	0.086	1.30	0.022	0.039	18.27	$5.05{\cdot}10^{-4}$	0.63	0.010
50	5.44	$7.91{\cdot}10^{-4}$	0.019	1.21	0.009	0.011	14.31	$3.17{\cdot}10^{-4}$	0.66	$1.86{\cdot}10^{-3}$
ACPS850-Z-D										
0	4.17	$4.85{\cdot}10^{-3}$	0.183	1.99	0.129	0.42	9.19	$6.81{\cdot}10^{-3}$	0.41	$8.90{\cdot}10^{-5}$
25	3.53	$3.45{\cdot}10^{-3}$	0.062	1.81	0.071	0.14	9.64	$3.37{\cdot}10^{-3}$	0.40	$8.69{\cdot}10^{-4}$
50	2.85	$2.08{\cdot}10^{-3}$	0.016	1.49	0.022	0.064	6.04	$1.38{\cdot}10^{-3}$	0.56	$1.36{\cdot}10^{-4}$
ACPS850-Z-W										
0	4.42	$4.53{\cdot}10^{-3}$	0.174	1.96	0.126	0.42	9.94	$6.28{\cdot}10^{-3}$	0.41	$6.13{\cdot}10^{-4}$
25	3.60	$3.36{\cdot}10^{-3}$	0.051	1.79	0.069	0.14	3.24	$3.11{\cdot}10^{-3}$	0.42	$1.75{\cdot}10^{-4}$
50	2.90	$2.05{\cdot}10^{-3}$	0.018	1.49	0.022	0.064	6.07	$1.36{\cdot}10^{-3}$	0.57	$2.48{\cdot}10^{-4}$

T (°C); $n_{m,L}$ and $n_{m,T}$ (mmol/g); K_L (1/mmHg), K_F (mmol/g·mmHg$^{1/nF}$), K_T (1/mmHg), n_F, t and ESS are dimensionless parameters

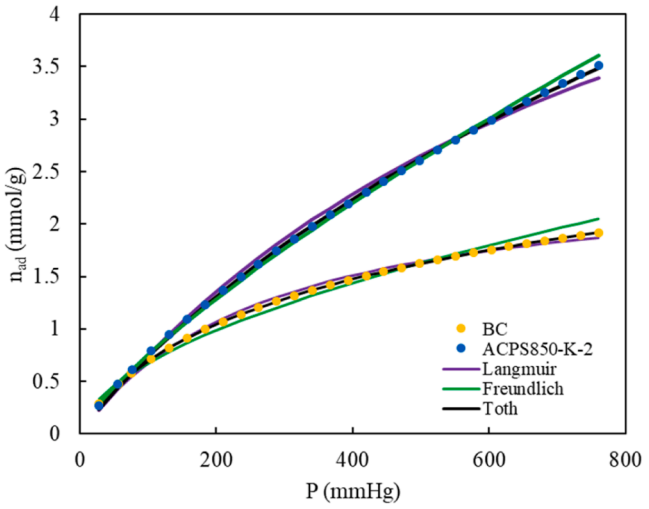

Fig. 9. Experimental CO_2 adsorption data at 25 °C for BC and ACPS850-K-2 and the corresponding fitting curves to Langmuir, Freundlich and Toth models.

especially for BC as above 600 mmHg Freundlich model deviates from the experimental data. However, Freundlich model best fitted ACPS600-K-4 equilibrium data at all temperatures essayed and those for ACPS850-K-4 at 25 and 50 °C.

Similarly, Table 10 shows for all carbons the isotherms parameters for N_2 adsorption at different temperatures and the respective error sum of squares (ESS).

The behavior is similar to that of CO_2 adsorption with a better fit to the Toth isotherm model in most cases, however, as expected the maximum adsorption capacity values are lower for N_2 adsorption due to the less affinity for this gas explained previously.

Regarding t parameter, a high variability among carbons and with changing temperature was found. The good fit to the Toth model shows that in general N_2 molecules were adsorbed in multimolecular layers because of adsorbent surface heterogeneity ($t \neq 1$), also when $t > 1$ lateral interactions between the adsorbed molecules are greater than the adsorptive potential [58]. However, for 0°C the behavior of BC, ACPS600-K-4, ACPS850-Z-D and ACPS850-Z-W carbons changed, t parameter is close to the unity, which means low heterogeneity and may be influenced by the poorer interactions between the N_2 and the surface [56].

3.4.4. CO_2/N_2 selectivity

The great CO_2 uptake ability of carbons previously found promotes the further assessment of their potential application in post combustion CO_2 capture. CO_2/N_2 selectivity is a very important parameter for adsorbent evaluation, and this was determined using single-component gas adsorption isotherms. From the obtained data, interesting information can be extracted regarding the apparent selectivity, or CO_2/N_2 selectivity, which was calculated as follows:

$$S_{CO_2/N_2} = \frac{n_{adCO_2}/P_{CO_2}}{n_{adN_2}/P_{N_2}} \quad (5)$$

where n_{adCO_2} and n_{adN_2} are the uptake capacities (mmol/g) of CO_2 and N_2, respectively, obtained from the isotherm that best fit experimental data at 0 °C. P_{CO_2} and P_{N_2} are the partial pressure of each component at a total pressure of 760 mmHg for a mixture CO_2/N_2 (15 % vol. CO_2).

As mentioned before, a preliminary estimation of the selectivity could be performed using the pure component equilibrium data for CO_2/N_2 separation. Nevertheless, it should be emphasized that the apparent selectivity calculated according to Eq. (5) can lead to conservative estimations since they are determined from the dynamic adsorption of pure components. According to González et al. [59] in a multicomponent system the adsorption of the weak adsorbate, this is nitrogen, could be considerably lower than when it is measured for a pure gas [9].

Table 11 summarizes the results obtained for the CO_2/N_2 selectivity determined by Eq. (5) and adsorption data obtained using the model that best fits the data based on the results shown in Tables 9 and 10, being BC and ACPS600-K-4 the carbons with higher selectivity. Table 12 shows the influence of temperature on selectivity for both materials, showing that selectivity increased with increasing temperature. Both CO_2 and N_2 uptake decreased with increasing temperature, which could be related with a physisorption process, as it was indicated above.

Since the apparent selectivity calculated represents a conservative

Table 10
Isotherms parameters for N_2 adsorption.

	Langmuir			Freundlich			Toth			
T	$n_{m,L}$	K_L	ESS_L	n_F	K_F	ESS_F	$n_{m,T}$	K_T	t	ESS_T
BC										
0	0.82	$7.99{\cdot}10^{-4}$	$1.39{\cdot}10^{-5}$	1.18	$1.19{\cdot}10^{-3}$	$2.12{\cdot}10^{-3}$	0.82	$8.12{\cdot}10^{-4}$	0.99	$9.18{\cdot}10^{-6}$
25	0.27	$1.61{\cdot}10^{-3}$	$2.13{\cdot}10^{-4}$	1.31	$1.07{\cdot}10^{-3}$	$2.18{\cdot}10^{-3}$	0.16	$2.19{\cdot}10^{-3}$	2.07	$1.36{\cdot}10^{-5}$
50	0.08	$4.15{\cdot}10^{-3}$	$3.58{\cdot}10^{-4}$	1.59	$1.12{\cdot}10^{-3}$	$1.35{\cdot}10^{-3}$	0.06	$3.39{\cdot}10^{-3}$	4.56	$7.64{\cdot}10^{-5}$
ACPS850-K-4										
0	2.17	$4.78{\cdot}10^{-4}$	$1.93{\cdot}10^{-5}$	1.11	$1.56{\cdot}10^{-3}$	$3.91{\cdot}10^{-3}$	13.7	$9.21{\cdot}10^{-5}$	0.48	$2.38{\cdot}10^{-4}$
25	0.71	$9.06{\cdot}10^{-4}$	$1.85{\cdot}10^{-4}$	1.19	$1.25{\cdot}10^{-3}$	$3.49{\cdot}10^{-3}$	12.7	$1.06{\cdot}10^{-4}$	0.31	$6.71{\cdot}10^{-4}$
50	0.25	$1.81{\cdot}10^{-3}$	$5.38{\cdot}10^{-4}$	1.35	$1.20{\cdot}10^{-3}$	$3.34{\cdot}10^{-3}$	13.9	$3.79{\cdot}10^{-4}$	0.18	$5.98{\cdot}10^{-5}$
ACPS600-K-4										
0	2.18	$4.7{\cdot}10^{-4}$	$2.02{\cdot}10^{-5}$	1.11	$1.53{\cdot}10^{-3}$	$3.92{\cdot}10^{-3}$	1.70	$5.93{\cdot}10^{-4}$	1.15	$1.10{\cdot}10^{-6}$
25	0.79	$7.91{\cdot}10^{-4}$	$7.41{\cdot}10^{-5}$	1.17	$1.12{\cdot}10^{-3}$	$2.37{\cdot}10^{-3}$	1.18	$5.89{\cdot}10^{-4}$	0.75	$1.20{\cdot}10^{-4}$
50	0.30	$1.48{\cdot}10^{-3}$	$2.80{\cdot}10^{-4}$	1.29	$1.02{\cdot}10^{-3}$	$2.92{\cdot}10^{-3}$	0.96	$8.55{\cdot}10^{-4}$	0.44	$5.73{\cdot}10^{-4}$
ACPS850-K-2										
0	2.84	$4.38{\cdot}10^{-4}$	$1.39{\cdot}10^{-6}$	1.10	$1.81{\cdot}10^{-3}$	$4.69{\cdot}10^{-3}$	8.09	$1.69{\cdot}10^{-4}$	0.63	$1.12{\cdot}10^{-4}$
25	1.27	$6.22{\cdot}10^{-4}$	$9.12{\cdot}10^{-5}$	1.14	$1.30{\cdot}10^{-3}$	$3.57{\cdot}10^{-3}$	1.76	$4.3{\cdot}10^{-4}$	1.22	$1.92{\cdot}10^{-6}$
50	0.54	$1.00{\cdot}10^{-3}$	$2.02{\cdot}10^{-3}$	1.21	$9.86{\cdot}10^{-4}$	$2.02{\cdot}10^{-3}$	1.47	$4.52{\cdot}10^{-4}$	0.55	$2.38{\cdot}10^{-3}$
ACPS850-Z-D										
0	1.45	$9.20{\cdot}10^{-4}$	$1.34{\cdot}10^{-5}$	1.21	$2.67{\cdot}10^{-3}$	$8.33{\cdot}10^{-3}$	1.55	$8.61{\cdot}10^{-4}$	0.96	$1.44{\cdot}10^{-6}$
25	0.83	$9.70{\cdot}10^{-4}$	$1.06{\cdot}10^{-4}$	1.22	$1.63{\cdot}10^{-3}$	$4.43{\cdot}10^{-3}$	0.67	$1.15{\cdot}10^{-3}$	1.17	$6.86{\cdot}10^{-5}$
50	0.38	$1.23{\cdot}10^{-3}$	$2.04{\cdot}10^{-4}$	1.26	$1.03{\cdot}10^{-3}$	$2.51{\cdot}10^{-3}$	0.22	$1.81{\cdot}10^{-3}$	1.92	$1.38{\cdot}10^{-5}$
ACPS850-Z-W										
0	1.43	$1.01{\cdot}10^{-3}$	$7.9{\cdot}10^{-6}$	1.23	$3.08{\cdot}10^{-3}$	$1.09{\cdot}10^{-2}$	1.40	$1.03{\cdot}10^{-3}$	1.02	$6.21{\cdot}10^{-4}$
25	0.73	$1.20{\cdot}10^{-3}$	$3.11{\cdot}10^{-4}$	1.26	$1.94{\cdot}10^{-3}$	$7.03{\cdot}10^{-3}$	0.48	$1.63{\cdot}10^{-3}$	1.57	$2.17{\cdot}10^{-5}$
50	0.31	$1.60{\cdot}10^{-3}$	$4.32{\cdot}10^{-4}$	1.32	$1.25{\cdot}10^{-3}$	$3.54{\cdot}10^{-3}$	0.19	$2.19{\cdot}10^{-3}$	2.35	$3.80{\cdot}10^{-5}$

T (°C); $n_{m,L}$ and $n_{m,T}$ (mmol/g); K_L (1/mmHg), K_F (mmol/g·mmHg$^{1/nF}$), K_T (1/mmHg); n_F, t and ESS are dimensionless parameters

Table 11
Calculated adsorption data of CO_2 and N_2 determined by the isotherm that best fit experimental data at 0°C and the corresponding values of apparent selectivity calculated for all carbons for a CO_2:N_2 (0.15:0.85) mixture.

Sample	n_{ad,CO_2} (mmol/g)	n_{ad,N_2} (mmol/g)	S_{CO_2/N_2}
BC	1.22 (T)	0.28 (T)	24.92
ACPS850-K-4	1.05 (T)	0.51 (L)	11.66
ACPS600-K-4	1.74 (F)	0.51 (T)	19.44
ACPS850-K-2	1.38 (T)	0.63 (L)	12.49
ACPS850-Z-D	1.51 (T)	0.54 (T)	15.87
ACPS850-Z-W	1.50 (T)	0.56 (L)	15.19

F: Freundlich; T: Toth; L: Langmuir.

Table 12
Apparent CO_2/N_2 selectivity, CO_2 and N_2 uptake capacity and IAST selectivity determined by the isotherm that best fit experimental data at 0°C for BC and ACPS600-K-4 carbons for a CO_2:N_2 (0.15:0.85) mixture.

Sample	Temperature (°C)	n_{ad,CO_2} (mmol/g)	n_{ad,N_2} (mmol/g)	S_{CO_2/N_2}	S_{IAST}
BC	0	1.22 (T)	0.28 (T)	24.92	562.03
	25	0.75 (T)	0.13 (T)	32.26	296.50
	50	0.39 (T)	0.06 (T)	36.74	34.46
ACPS600-K-4	0	1.67 (F)	0.51 (T)	19.44	132.87
	25	0.97 (F)	0.37 (L)	20.74	39.73
	50	0.53 (F)	0.14 (L)	26.40	34.65

F: Freundlich; T: Toth; L: Langmuir.

approximation, adsorption selectivity was determined also using the ideal adsorbed solution theory (IAST) and is represented in Fig. 10. IAST is a widely used method for predicting the adsorption equilibrium for components in a mixture using only single component adsorption data at the same temperature and with the same adsorbent. This theory is based on three assumptions: (1) the same surface area is accessible to all adsorbates; (2) the adsorbent is inert; (3) the multicomponent mixture acts as an ideal solution (the strength of interaction is equal between all molecules) at a constant spreading pressure, usually defined as the negative value of the surface tension, and temperature [60,61].

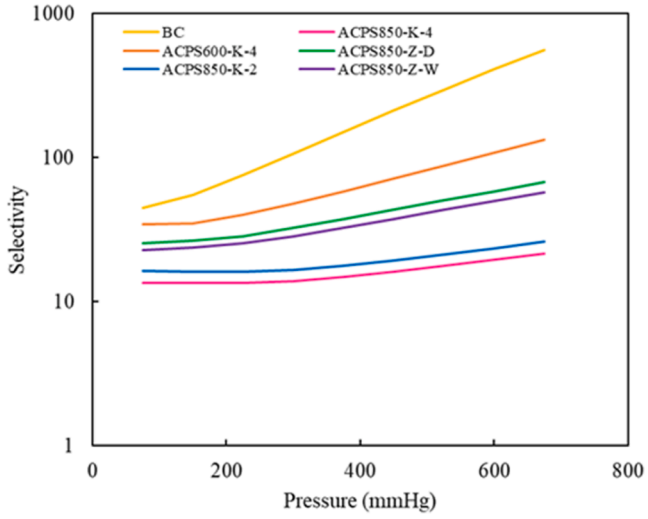

Fig. 10. IAST adsorption selectivity of CO_2 over N_2 calculated at 0 °C for a binary mixture with 15 % CO_2 for all carbons prepared.

From the values of selectivity estimated, it can be confirmed that in all cases CO_2 is preferentially adsorbed over N_2 as reported by Chowdhury & Balasubramanian [56] for other activated carbons derived from biomass, although higher selectivity values were obtained in the present work for carbons based on pine sawdust.

Fig. 10 shows the effect of pressure on CO_2/N_2 selectivity. All materials presented the same trend, however, the effect of pressure on selectivity was more significant for the biochar than for the activated carbons. At higher pressure more CO_2 and N_2 are present, therefore, the competition for adsorption sites intensifies. However, the selectivity significantly raised for the non-activated carbon due to a higher affinity for CO_2 that can be explained by the presence of more functional groups compared to activated carbons, which showed a more homogeneous surface from a chemical point of view, and therefore only a slight increase in selectivity [62].

Moreover, the fundamental role of microporosity on selectivity was

demonstrated as observed in Fig. 11 as an increase in microporosity percentage (%) led to a significant selectivity increase.

Additionally, a considerable decrease in selectivity was observed for those materials with higher surface areas (Fig. 12), which is also related to the previous results. Thus, the activation process with both activated agents, $ZnCl_2$ and KOH, led to an increase in the surface area (and also in the amount of CO_2 adsorbed) but to the loss of surface functional groups and microporosity (mainly in the ultramicroporosity range).

Regarding the selectivity estimated by applying the IAST, an opposite effect of temperature was observed (Table 12) as it decreased with increasing temperature, indicating the importance of competitive adsorption of CO_2/N_2. This finding is in agreement with previous studies employing other types of carbonaceous materials which concluded that CO_2 adsorption is more temperature dependent than N_2 adsorption [63].

3.5. Heat of adsorption

To better understand the behavior of the activated carbons prepared in the separation of carbon dioxide from binary streams, the isosteric heat of CO_2 adsorption (Q_{st}) was determined. The heat of adsorption is a measure of the surface affinity toward CO_2 and indicates the strength of interaction between molecules of the adsorbate and the surface of the adsorbent.

It was calculated using different carbon dioxide loadings which allowed the evaluation of changes in the adsorption mechanisms or in the adsorption sites during the surface coverage process, and the Clausius-Clapeyron equation (Eq. (6)) [1,2]:

$$Q_{st} = R\left[\frac{\partial \ln P}{\partial (1/T)}\right]_{\theta} \quad (6)$$

where Q_{st} (kJ/mol) is the heat of adsorption, R is the ideal gas constant ($8.314 \cdot 10^{-3}$ kJ/mol K), θ is the CO_2 surface coverage at a pressure P (Pa) and temperature T (K). A plot of ln P versus 1/T provides a straight line with a slope of Q_{st}. Also, Toth isotherm parameters were employed (Table 9) since, in general and, as explained previously, this model showed the best fit for the experimental equilibrium data.

Additionally, the results obtained allowed to analyze the influence of the type of material and the amount of gas adsorbed on the CO_2 adsorption isosteric heat as shown in Fig. 13.

It can be observed that, for all materials, the heats of adsorption were low, in the range from 14 to 27 kJ/mol and depended little on the amount of CO_2 adsorbed. Then, it can be concluded that the interactions between the materials and CO_2 correspond to a physical adsorption which implies that these carbons will require a low amount of energy for regeneration which is of great relevance when applying these materials

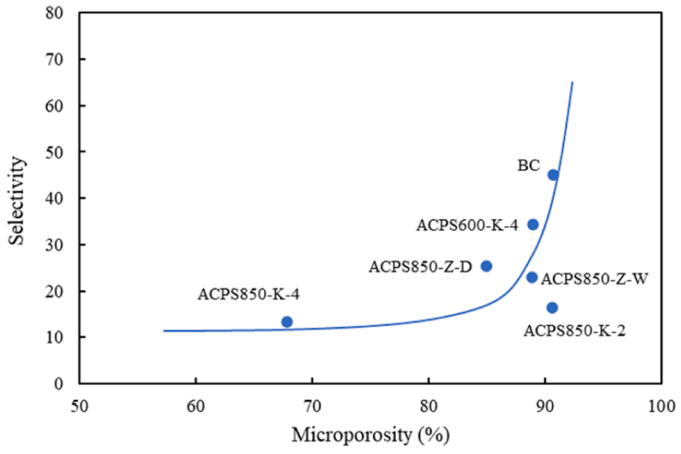

Fig. 11. Influence of the microporosity percentage on the selectivity determined at 0 °C and 75 mmHg.

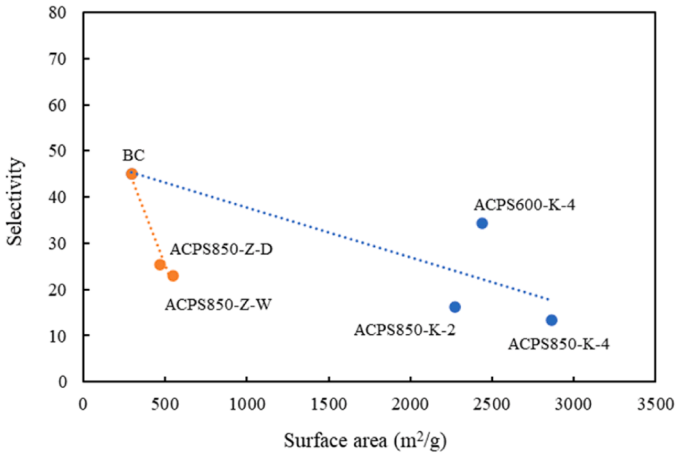

Fig. 12. Influence of the surface area on the selectivity determined at 0 °C and 75 mmHg.

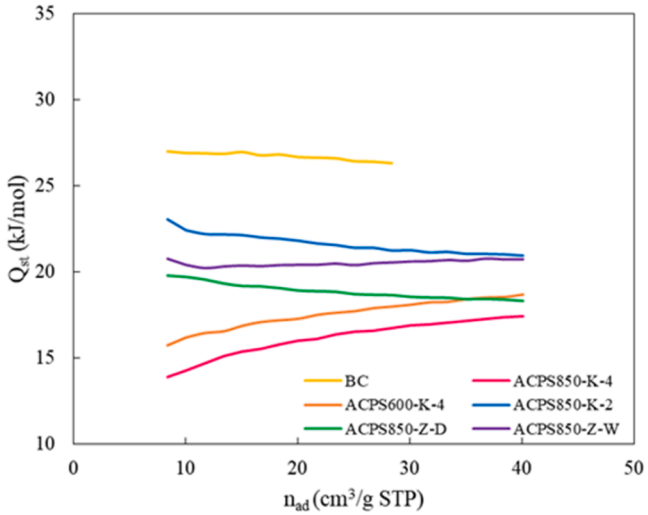

Fig. 13. Influence of amount adsorbed upon isosteric heat of adsorption for CO_2 on the different carbons used.

for the continuous separation of CO_2 from gaseous streams since the costs of the desorption stage will be lower.

On the other hand, the heat of adsorption of the carbons prepared are of the same order than those reported by Manyà et al. [9] for other porous carbons. On the contrary, some previous studies [64,65] showed higher values of the heat of adsorption at low surface coverage related with the presence of active centers on the adsorbent surface that caused a chemical adsorption. However, as mentioned before, for most of the materials, except for the carbons activated with KOH at 1:4 (w/w), there is a low influence of the amount adsorbed upon the heat of adsorption (Fig. 13), which can be related to a low surface heterogeneity.

Among the carbons used, BC presented the highest heat of CO_2 adsorption which is in agreement with the presence of more functional groups on the surface since the activation step did not take place. Regarding the other materials, the carbons activated with the highest amount of KOH, ACPS850-K-4 and ACPS600-K-4, are those that showed the lowest heat of adsorption due to a stronger activation (high temperature and/or BC/KOH ratio) that led to a more homogeneous adsorbent surface.

Besides, different trends of the isosteric heat with the amount of CO_2 adsorbed were observed. For BC, ACPS850-K-2 and ACPS850-Z-D the heat of adsorption decreased with increasing the amount adsorbed, while for ACPS850-K-4 and ACPS600-K-4 increased, and ACPS-850-Z-W

did not show changes. This variation in the trend indicates that small size micropores in carbons are occupied first by CO_2 molecules, which indicates heterogeneous energetic properties of adsorption [8]. On the other hand, the decrease in the isosteric heat can be attributed to the heterogeneous characteristics of the carbon's surface, which implies strong interactions of CO_2 with the carbon surface and negligible intermolecular interaction between CO_2 molecules on the carbon's surface can be assumed [1,66]. Previous studies presented a similar behavior and reported that an increase in isosteric heat could be related to the reinforced intermolecular interaction between the adsorbent and the adsorbate. This behavior implies the multilayer adsorption of CO_2 over the adsorbent.

4. Conclusions

Pine sawdust derived biochar and activated carbons with good CO_2 adsorption properties were successfully prepared through carbonization and activation with KOH or $ZnCl_2$. The experimental results demonstrated that the activating agent had a substantial effect on carbon porosity. All carbons presented an amorphous structure with different degrees of graphitization, C and O as the main components and a branch of functional groups. The microporosity percentage decreased in the next order BC > ACPS850-Z-D > ACPS600-K-4 >ACPS850-Z-W > ACPS850-K-2 >ACPS850-K-4, however, a high microporosity did not imply a high BET surface area. For KOH activation CO_2 uptake improved at moderate conditions (600 ºC). CO_2 uptake can be related with several material characteristics such as micropore geometry and surface chemistry. ACPS600-K-4 displayed the largest CO_2 uptake (5.79 mmol/g at 0 °C and 3.43 mmol/g at 25 °C and 750 mmHg) due to the combination of a high microporosity (89 %) and a high surface area (2437 m^2/g). Moreover, all carbons showed preferential sorption for CO_2 over N_2 and there was a negative effect of temperature on CO_2 adsorption capacity. Toth isotherm model fitted the adsorption experimental data better than Langmuir and Freundlich models in most cases. Furthermore, apparent selectivity and IAST estimated values indicated that BC followed by ACPS600-K-4 showed the best CO_2/N_2 selectivity allowing to reach high purity gas stream. Regarding the heat of CO_2 adsorption, BC presented the highest value which is related with the presence of more functional groups on the surface since the activation step did not take place and in agreement with the high estimated selectivity for BC though this material presents the lowest surface area. On the basis of the results discussed in this work and taking into account various parameters such as the amount of CO_2 adsorbed and the heat of adsorption, ACPS600-K-4 exhibited the best performance since it allowed to reach the highest carbon dioxide uptake, it has the second highest selectivity value combined with the second lowest heat of adsorption. All these findings make this material the most promising option with the appropriate characteristics to be used for CO_2 capture. The results obtained are very promising for the selective separation of CO_2 taking into account that the carbon precursor used is an industrial waste that must be managed.

CRediT authorship contribution statement

Catarina H. Pimentel: Investigation, Data curation, Validation, Visualization, Writing – original draft (catarinahelena.dasilveira@rai.usc.es). **L. Díaz-Fernández**: Investigation, Data curation, Validation, Conducted the experiments and data/evidence collection (lidiadife@gmail.com). **Diego Gómez-Díaz**: Conceptualization, Methodology, Supervision, Verified the accuracy of the results, Funding acquisition, Writing—review & editing (diego.gomez@usc.es). **M. Sonia Freire**: Conceptualization, Methodology, Supervision, Verified the accuracy of the results, Funding acquisition, Writing—review & editing (mariasonia.freire@usc.es). **Julia González-Álvarez**: Conceptualization, Methodology, Supervision, Funding acquisition, Writing—review & editing (julia.gonzalez@usc.es).

Declaration of Competing Interest

The authors declare that they have no known competing financial interests or personal relationships that could have appeared to influence the work reported in this paper.

Data availability

Data will be made available on request.

Acknowledgments

This work was supported by Xunta de Galicia (ED431B 2020/039) and by MCIN/AEI /10.13039/501100011033 / FEDER, UE (PID2021–122923NB-I00). Authors would like to thank the use of RIAIDT-USC analytical facilities.

Appendix A. Supporting information

Supplementary data associated with this article can be found in the online version at doi:10.1016/j.jece.2023.111378.

References

[1] J. Serafin, U. Narkiewicz, A.W. Morawski, R.J. Wróbel, B. Michalkiewicz, Highly microporous activated carbons from biomass for CO_2 capture and effective micropores at different conditions, J. CO_2 Util. 18 (2017) 73–79, https://doi.org/10.1016/j.jcou.2017.01.006.

[2] G. Sethia, A. Sayari, Comprehensive study of ultra-microporous nitrogen-doped activated carbon for CO_2 capture, Carbon 93 (2015) 68–80, https://doi.org/10.1016/j.carbon.2015.05.017.

[3] I.S. Ismail, N.A. Rashidi, S. Yusup, Production and characterization of bamboo-based activated carbon through single-step H3PO4 activation for CO_2 capture, Environ. Sci. Pollut. Res. 29 (2022) 12434–12440, https://doi.org/10.1007/s11356-021-15030-x.

[4] N. Abuelnoor, A. AlHajaj, M. Khaleel, L.F. Vega, M.R.M. Abu-Zahra, Activated carbons from biomass-based sources for CO_2 capture applications, Chemosphere 282 (2021), 131111, https://doi.org/10.1016/j.chemosphere.2021.131111.

[5] A. Sarwar, M. Ali, A. Hussain, A. Nawar, A. Waqas, R. Liaquat, S. Raza, M. Asjid, Synthesis and characterization of biomass-derived surface-modified activated carbon for enhanced CO2 adsorption, J. CO_2 Util. 46 (2021), 101476, https://doi.org/10.1016/j.jcou.2021.101476.

[6] S. Deng, H. Wei, T. Chen, B. Wang, J. Huang, G. Yu, Superior CO_2 adsorption on pine nut shell-derived activated carbons and the effective micropores at different temperatures, Chem. Eng. J. 253 (2014) 46–54, https://doi.org/10.1016/j.cej.2014.04.115.

[7] W. Hao, E. Björkman, M. Lilliestråle, N. Hedin, Activated carbons prepared from hydrothermally carbonized waste biomass used as adsorbents for CO 2, Appl. Energy 112 (2013) 526–532, https://doi.org/10.1016/j.apenergy.2013.02.028.

[8] G. Huang, Y. Liu, X. Wu, J. Cai, Activated carbons prepared by the KOH activation of a hydrochar from garlic peel and their CO 2 adsorption performance, N. Carbon Mater. 34 (2019) 247–257, https://doi.org/10.1016/S1872-5805(19)60014-4.

[9] J.J. Manyà, B. González, M. Azuara, G. Arner, Ultra-microporous adsorbents prepared from vine shoots-derived biochar with high CO_2 uptake and CO_2/N2 selectivity, Chem. Eng. J. 345 (2018) 631–639, https://doi.org/10.1016/j.cej.2018.01.092.

[10] C.I. Orozco, M.S. Freire, D. Gómez-díaz, J. González-álvarez, Removal of copper from aqueous solutions by biosorption onto pine sawdust, 32, 2023. ⟨https://doi.org/10.1016/j.scp.2023.101016⟩.

[11] K.A. Adegoke, O.O. Adesina, O.A. Okon-Akan, O.R. Adegoke, A.B. Olabintan, O. A. Ajala, H. Olagoke, N.W. Maxakato, O.S. Bello, Sawdust-biomass based materials for sequestration of organic and inorganic pollutants and potential for engineering applications, Curr. Res. Green Sustain. Chem. 5 (2022), 100274, https://doi.org/10.1016/j.crgsc.2022.100274.

[12] S. Mallakpour, F. Sirous, C.M. Hussain, Sawdust, a versatile, inexpensive, readily available bio-waste: from mother earth to valuable materials for sustainable remediation technologies, Adv. Colloid Interface Sci. 295 (2021), 102492, https://doi.org/10.1016/j.cis.2021.102492.

[13] S. Velusamy, A. Roy, S. Sundaram, T. Kumar Mallick, A review on heavy metal ions and containing dyes removal through graphene oxide-based adsorption strategies for textile wastewater treatment, Chem. Rec. 21 (2021) 1570–1610, https://doi.org/10.1002/tcr.202000153.

[14] C. Quan, R. Su, N. Gao, Preparation of activated biomass carbon from pine sawdust for supercapacitor and CO_2 capture, Int. J. Energy Res. 44 (2020) 4335–4351, https://doi.org/10.1002/er.5206.

[15] A.D. Igalavithana, S.W. Choi, J. Shang, A. Hanif, P.D. Dissanayake, D.C.W. Tsang, J.H. Kwon, K.B. Lee, Y.S. Ok, Carbon dioxide capture in biochar produced from pine sawdust and paper mill sludge: effect of porous structure and surface

chemistry, Sci. Total Environ. 739 (2020), 139845, https://doi.org/10.1016/j.scitotenv.2020.139845.
[16] C.H. Pimentel, M.S. Freire, D. Gómez-Díaz, J. González-Álvarez, Preparation of activated carbon from pine (Pinus radiata) sawdust by chemical activation with zinc chloride for wood dyes adsorption, Biomass Convers. Biorefin. (2023), https://doi.org/10.1007/s13399-023-04138-4.
[17] O.E. Eleri, K.U. Azuatalam, M.W. Minde, A.M. Trindade, N. Muthuswamy, F. Lou, Z. Yu, Towards high-energy-density supercapacitors via less-defects activated carbon from sawdust, Electrochim. Acta 362 (2020), 137152, https://doi.org/10.1016/j.electacta.2020.137152.
[18] M.B. Ahmed, M.A. Hasan Johir, J.L. Zhou, H.H. Ngo, L.D. Nghiem, C. Richardson, M.A. Moni, M.R. Bryant, Activated carbon preparation from biomass feedstock: clean production and carbon dioxide adsorption, J. Clean. Prod. 225 (2019) 405–413, https://doi.org/10.1016/j.jclepro.2019.03.342.
[19] E. Dautzenberg, S. van Hurne, M.M.J. Smulders, L.C.P.M. de Smet, GraphIAST: a graphical user interface software for ideal adsorption solution theory (IAST) calculations, Comput. Phys. Commun. 280 (2022), 108494, https://doi.org/10.1016/j.cpc.2022.108494.
[20] M.A. Yahya, Z. Al-Qodah, C.W.Z. Ngah, Agricultural bio-waste materials as potential sustainable precursors used for activated carbon production: a review, Renew. Sustain. Energy Rev. 46 (2015) 218–235, https://doi.org/10.1016/j.rser.2015.02.051.
[21] M. Danish, T. Ahmad, A review on utilization of wood biomass as a sustainable precursor for activated carbon production and application, Renew. Sustain. Energy Rev. 87 (2018) 1–21, https://doi.org/10.1016/j.rser.2018.02.003.
[22] Ö. Akçakal, M. Şahin, M. Erdem, Synthesis and characterization of high-quality activated carbons from hard-shelled agricultural wastes mixture by zinc chloride activation, Chem. Eng. Commun. 206 (2019) 888–897, https://doi.org/10.1080/00986445.2018.1534231.
[23] A. Tomczyk, Z. Sokołowska, P. Boguta, Biomass type effect on biochar surface characteristic and adsorption capacity relative to silver and copper, Fuel 278 (2020), https://doi.org/10.1016/j.fuel.2020.118168.
[24] Z. Heidarinejad, M.H. Dehghani, M. Heidari, G. Javedan, I. Ali, M. Sillanpää, Methods for preparation and activation of activated carbon: a review, Environ. Chem. Lett. 18 (2020) 393–415, https://doi.org/10.1007/s10311-019-00955-0.
[25] R. Chikri, N. Elhadiri, M. Benchanaa, Y. El maguana, Efficiency of sawdust as low-cost adsorbent for dyes removal, J. Chem. 2020 (2020) 1–17, https://doi.org/10.1155/2020/8813420.
[26] D. Angin, E. Altintig, T.E. Köse, Influence of process parameters on the surface and chemical properties of activated carbon obtained from biochar by chemical activation, Bioresour. Technol. 148 (2013) 542–549, https://doi.org/10.1016/J.BIORTECH.2013.08.164.
[27] Z. Zhang, X. Luo, Y. Liu, P. Zhou, G. Ma, Z. Lei, L. Lei, A low cost and highly efficient adsorbent (activated carbon) prepared from waste potato residue, J. Taiwan Inst. Chem. Eng. 49 (2015) 206–211, https://doi.org/10.1016/J.JTICE.2014.11.024.
[28] M. Erdem, R. Orhan, M. Şahin, E. Aydın, Preparation and characterization of a novel activated carbon from vine shoots by ZnCl2 activation and investigation of its rifampicine removal capability, Water Air Soil Pollut. 227 (2016) 1–14, https://doi.org/10.1007/S11270-016-2929-5/FIGURES/11.
[29] R.L. Tseng, S.K. Tseng, Characterization and use of high surface area activated carbons prepared from cane pith for liquid-phase adsorption, J. Hazard. Mater. 136 (2006) 671–680, https://doi.org/10.1016/J.JHAZMAT.2005.12.048.
[30] A.H. Basta, V. Fierro, H. El-Saied, A. Celzard, 2-Steps KOH activation of rice straw: an efficient method for preparing high-performance activated carbons, Bioresour. Technol. 100 (2009) 3941–3947, https://doi.org/10.1016/J.BIORTECH.2009.02.028.
[31] A.N.A. El-Hendawy, An insight into the KOH activation mechanism through the production of microporous activated carbon for the removal of Pb2+ cations, Appl. Surf. Sci. 255 (2009) 3723–3730, https://doi.org/10.1016/J.APSUSC.2008.10.034.
[32] M. Jaouadi, Characterization of activated carbon, wood sawdust and their application for boron adsorption from water, Int. Wood Prod. J. 12 (2021) 22–33, https://doi.org/10.1080/20426445.2020.1785605.
[33] S. Álvarez-Torrellas, M. Muñoz, J.A. Zazo, J.A. Casas, J. García, Synthesis of high surface area carbon adsorbents prepared from pine sawdust-Onopordum acanthium L. for nonsteroidal anti-inflammatory drugs adsorption, J. Environ. Manag. 183 (2016) 294–305, https://doi.org/10.1016/j.jenvman.2016.08.077.
[34] E. Köseoğlu, C. Akmil-Başar, Preparation, structural evaluation and adsorptive properties of activated carbon from agricultural waste biomass, Adv. Powder Technol. 26 (2015) 811–818, https://doi.org/10.1016/j.apt.2015.02.006.
[35] Q. Li, S. Liu, W. Peng, W. Zhu, L. Wang, F. Chen, J. Shao, X. Hu, Preparation of biomass-derived porous carbons by a facile method and application to CO_2 adsorption, J. Taiwan Inst. Chem. Eng. 116 (2020) 128–136, https://doi.org/10.1016/j.jtice.2020.11.001.
[36] Q. Pu, J. Zou, J. Wang, S. Lu, P. Ning, L. Huang, Q. Wang, Systematic study of dynamic CO_2 adsorption on activated carbons derived from different biomass, J. Alloy. Compd. 887 (2021), 161406, https://doi.org/10.1016/j.jallcom.2021.161406.
[37] V. Benedetti, E. Cordioli, F. Patuzzi, M. Baratieri, CO_2 Adsorption study on pure and chemically activated chars derived from commercial biomass gasifiers, J. CO_2 Util. 33 (2019) 46–54, https://doi.org/10.1016/j.jcou.2019.05.008.
[38] E. Yagmur, Y. Gokce, S. Tekin, N.I. Semerci, Z. Aktas, Characteristics and comparison of activated carbons prepared from oleaster (Elaeagnus angustifolia L.) fruit using KOH and ZnCl2, Fuel 267 (2020), 117232, https://doi.org/10.1016/j.fuel.2020.117232.
[39] Z. Liu, Y. Huang, Z. Guangjie, Preparation and characterization of activated carbon fibers from liquefied wood by ZnCl2 activation, BioResources 11 (2016) 3178–3190, https://doi.org/10.15376/biores.11.2.3178-3190.
[40] V. Siipola, T. Tamminen, A. Källi, R. Lahti, H. Romar, K. Rasa, R. Keskinen, J. Hyväluoma, M. Hannula, H. Wikberg, Effects of biomass type, carbonization process, and activation method on the properties of bio-based activated carbons, BioResources 13 (2019) 5976–6002, https://doi.org/10.15376/biores.13.3.5976-6002.
[41] S. Marzeddu, M.A. Décima, L. Camilli, M.P. Bracciale, V. Genova, L. Paglia, F. Marra, M. Damizia, M. Stoller, A. Chiavola, M.R. Boni, Physical-chemical characterization of different carbon-based sorbents for environmental applications, Materials 15 (2022) 1–29, https://doi.org/10.3390/ma15207162.
[42] N.A. Rashidi, S. Yusup, Biochar as potential precursors for activated carbon production: parametric analysis and multi-response optimization, Environ. Sci. Pollut. Res. 27 (2020) 27480–27490, https://doi.org/10.1007/s11356-019-07448-1.
[43] Y. Tadjenant, N. Dokhan, A. Barras, A. Addad, R. Jijie, S. Szunerits, R. Boukherroub, Graphene oxide chemically reduced and functionalized with KOH-PEI for efficient Cr(VI) adsorption and reduction in acidic medium, Chemosphere 258 (2020), 127316, https://doi.org/10.1016/j.chemosphere.2020.127316.
[44] S. Shi, Y. Liu, Nitrogen-doped activated carbons derived from microalgae pyrolysis by-products by microwave/KOH activation for CO_2 adsorption, Fuel 306 (2021), 121762, https://doi.org/10.1016/j.fuel.2021.121762.
[45] Y.J. Zhang, Z.J. Xing, Z.K. Duan, M. Li, Y. Wang, Effects of steam activation on the pore structure and surface chemistry of activated carbon derived from bamboo waste, Appl. Surf. Sci. 315 (2014) 279–286, https://doi.org/10.1016/j.apsusc.2014.07.126.
[46] M. Thommes, K. Kaneko, A.V. Neimark, J.P. Olivier, F. Rodriguez-Reinoso, J. Rouquerol, K.S.W. Sing, Physisorption of gases, with special reference to the evaluation of surface area and pore size distribution (IUPAC technical report, Pure Appl. Chem. 87 (2015) 1051–1069, https://doi.org/10.1515/pac-2014-1117.
[47] I. Durán, F. Rubiera, C. Pevida, Separation of CO_2 in a solid waste management incineration facility using activated carbon derived from pine sawdust, Energies 10 (2017), https://doi.org/10.3390/en10060827.
[48] L. Domínguez-Ramos, A. Prieto-Estalrich, G. Malucelli, D. Gómez-Díaz, M.S. Freire, M. Lazzari, J. González-álvarez, N- and S-doped carbons derived from polyacrylonitrile for gases separation, Sustain 14 (2022) 3760, https://doi.org/10.3390/SU14073760.
[49] R. Janu, V. Mrlik, D. Ribitsch, J. Hofman, P. Sedláček, L. Bielská, G. Soja, Biochar surface functional groups as affected by biomass feedstock, biochar composition and pyrolysis temperature, Carbon Resour. Convers. 4 (2021) 36–46, https://doi.org/10.1016/j.crcon.2021.01.003.
[50] K. Li, S. Tian, J. Jiang, J. Wang, X. Chen, F. Yan, Pine cone shell-based activated carbon used for CO_2 adsorption, J. Mater. Chem. A. 4 (2016) 5223–5234, https://doi.org/10.1039/C5TA09908K.
[51] C. Ma, J. Bai, M. Demir, X. Hu, S. Liu, L. Wang, Water chestnut shell-derived N/S-doped porous carbons and their applications in CO_2 adsorption and supercapacitor, Fuel 326 (2022), 125119, https://doi.org/10.1016/j.fuel.2022.125119.
[52] T. Lu, J. Bai, M. Demir, X. Hu, J. Huang, L. Wang, Synthesis of potassium Bitartrate-derived porous carbon via a facile and self-activating strategy for CO_2 adsorption application, Sep. Purif. Technol. 296 (2022), 121368, https://doi.org/10.1016/j.seppur.2022.121368.
[53] J. Bai, J. Huang, Q. Yu, M. Demir, F.H. Gecit, B.N. Altay, L. Wang, X. Hu, One-pot synthesis of self S-doped porous carbon for efficient CO_2 adsorption, Fuel Process. Technol. 244 (2023), 107700, https://doi.org/10.1016/j.fuproc.2023.107700.
[54] Q. Yu, J. Bai, J. Huang, M. Demir, A.A. Farghaly, P. Aghamohammadi, X. Hu, L. Wang, One-pot synthesis of melamine formaldehyde resin-derived N-doped porous carbon for CO_2 capture application, Molecules 28 (2023), https://doi.org/10.3390/molecules28041772.
[55] K.A. Babatunde, B.M. Negash, S.R. Jufar, T.Y. Ahmed, M.R. Mojid, Adsorption of gases on heterogeneous shale surfaces: a review, J. Pet. Sci. Eng. 208 (2022), 109466, https://doi.org/10.1016/J.PETROL.2021.109466.
[56] S. Chowdhury, R. Balasubramanian, Three-dimensional graphene-based porous adsorbents for postcombustion CO_2 capture, Ind. Eng. Chem. Res. 55 (2016) 7906–7916, https://doi.org/10.1021/acs.iecr.5b04052.
[57] M. Mabuza, K. Premlall, M.O. Daramola, Modelling and thermodynamic properties of pure - CO 2 and flue gas sorption data on South African coals using Langmuir, Freundlich, Temkin, and extended Langmuir isotherm models, Int. J. Coal Sci. Technol. (2022), https://doi.org/10.1007/s40789-022-00515-y.
[58] A.P. Terzyk, J. Chatłas, P.A. Gauden, G. Rychlicki, P. Kowalczyk, Developing the solution analogue of the Toth adsorption isotherm equation, J. Colloid Interface Sci. 266 (2003) 473–476, https://doi.org/10.1016/S0021-9797(03)00569-1.
[59] A.S. González, M.G. Plaza, F. Rubiera, C. Pevida, Sustainable biomass-based carbon adsorbents for post-combustion CO_2 capture, Chem. Eng. J. 230 (2013) 456–465, https://doi.org/10.1016/J.CEJ.2013.06.118.
[60] A.L. Myers, J.M. Prausnitz, Thermodynamics of mixed-gas adsorption, AIChE J. 11 (1965) 121–127, https://doi.org/10.1002/AIC.690110125.
[61] N.F. Cessford, N.A. Seaton, T. Dü, Evaluation of ideal adsorbed solution theory as a tool for the design of metal−organic framework, Materials (2012), https://doi.org/10.1021/ie202219w.
[62] W. Lu, W.M. Verdegaal, J. Yu, P.B. Balbuena, H.K. Jeong, H.C. Zhou, Building multiple adsorption sites in porous polymer networks for carbon capture applications, Energy Environ. Sci. 6 (2013) 3559–3564, https://doi.org/10.1039/C3EE42226G.
[63] C. Landaverde-Alvarado, A.J. Morris, S.M. Martin, Gas sorption and kinetics of CO_2 sorption and transport in a polymorphic microporous MOF with open Zn (II)

coordination sites, J. CO_2 Util. 19 (2017) 40–48, https://doi.org/10.1016/J.JCOU.2017.01.029.

[64] L.B. Sun, Y.H. Kang, Y.Q. Shi, Y. Jiang, X.Q. Liu, Highly selective capture of the greenhouse gas CO_2 in polymers, ACS Sustain. Chem. Eng. 3 (2015) 3077–3085, https://doi.org/10.1021/acssuschemeng.5b00544.

[65] C. Xu, Adsorption of CO_2 on a micro-/mesoporous polyimine modified with tris (2-aminoethyl) amine, J. Mater. Chem. A 3 (2015) 16229–16234.

[66] Y. Guo, C. Tan, J. Sun, W. Li, J. Zhang, C. Zhao, Porous activated carbons derived from waste sugarcane bagasse for CO_2 adsorption, Chem. Eng. J. 381 (2020), 122736, https://doi.org/10.1016/j.cej.2019.122736.